Accepted draft of the journal paper to be published in Philosophical Magazine 2005: Special Issue in Honor of SES 2003 Eringen Medalist G. Maugin.

Magnetic Field-Induced Martensitic Variant Reorientation in Magnetic Shape Memory Alloys

Björn Kiefer and Dimitris C. Lagoudas*

Department of Aerospace Engineering, Texas A&M University
H. R. Bright Building 3141 TAMU, College Station, TX 77843-3141, USA.

Dedicated to Professor Gerard Maugin
on the occasion of his receiving of the 2003 SES A. C. Eringen Medal

Abstract

The magnetically induced martensitic variant reorientation process under applied mechanical load in magnetic shape memory alloys (MSMAs) is considered. Of particular interest is the associated nonlinear and hysteretic macroscopic strain response under variable applied magnetic field in the presence of stress, also known as the magnetic shape memory effect (MSME). A thermodynamically consistent phenomenological constitutive model is derived which captures the magnetic shape memory effect caused by the martensitic variant reorientation process, using internal state variables, which are chosen in consideration of the crystallographic and magnetic microstructure. The magnetic contributions to the free energy function considered in this work are the Zeeman energy and the magnetocrystalline anisotropy energy. Activation functions for the onset and termination of the reorientation process are formulated and evolution equations for the internal state variables are derived. The model is applied to a 2-D special case in which the application of a transverse magnetic field produces axial reorientation strain in a NiMnGa single crystal specimen under a constant compressive axial stress. It is explicitly shown how the model parameters are obtained from experimental data. Model predictions of magnetic field-reorientation strain hysteresis loops under different applied stresses are discussed.

Keywords: magnetic shape memory alloys, magnetic shape memory effect, magnetic field-induced strain, martensitic variant reorientation, stress-magnetic field phase diagram.

Contents

*Corresponding Author. For further information please contact: lagoudas@aero.tamu.edu.

1 Introduction

Shape memory alloys (SMAs) have been an important member of the class of active materials for at least two decades now. They have successfully been used in actuator and sensor design as well as biomedical and numerous other technological applications. The large strain of 6–10% these materials exhibit when being subjected to thermal or mechanical load, is caused by the change in crystallography associated with a reversible austenite to martensite phase transformation. Magnetic shape memory alloys have more recently emerged as an interesting addition to this class of materials. In addition to the strains originating from temperature or stress controlled conventional shape memory behavior, large strains can be produced in these alloys under the external application of moderate magnetic fields. The macroscopically observable strain induced in MSMA is caused by the microstructural rearrangement of martensitic variants. Since the crystallographic variants of martensite have different preferred magnetization directions, applied magnetic fields can be used to select certain variants over others, resulting in the macroscopic shape change. The constitutive response is nonlinear and hysteretic, which gives the material interesting characteristics in terms of possible applications. In principle, under extreme conditions, the austenite to martensite phase transformation can also be induced in MSMAs under the application of magnetic fields. However, if the induction of phase transformation under magnetic fields is not facilitated by cooling the necessary magnetic field strength levels are usually very high. The variant reorientation process provides a technologically more attractive way of producing large inelastic strains by means of magnetic fields in these materials.

The main focus of this paper is the *magnetic field-induced martensitic variant reorientation* in MSMAs, which has also been termed *magnetostriction of martensite*, the *magnetic shape memory effect* (MSME), the *ferromagnetic shape memory effect* (FMSME) or the *magnetic field-induced variant rearrangement*. The first extensive account of the magnetic shape memory effect was given by Ullakko et al. (1996). They reported strains of nearly 0.2%, found in experiments on unstressed NiMnGa single crystals. Extensive experimental work on off-stoichiometric intermetallic compounds near the composition Ni_2MnGa have yielded larger field-induced strains of 6% (Murray et al., 2000a) and up to 10% (O'Handley et al., 2003; Sozinov et al., 2003) in single crystals. Next to the investigation of different compositions, the maximum reorientation strain levels have been increased through thermo-mechanical treatments and the utilization of a better understanding of the crystallographic structure of magnetic shape memory alloys. For simplicity, these compositions will collectively be referred to as NiMnGa in this paper, unless a specific alloy is discussed. A second alloy, FePd, has been investigated in detail (Cui et al., 2004; James and Wuttig, 1998; Shield, 2003; Yamamoto et al., 2004), and several additional material systems have also been tested, such as FeNiCoTi, FePt, CoNiGa, NiMnAl, among others (Murray et al., 1999; Fujita et al., 2000; Kakeshita et al., 2000; Wuttig et al., 2000, 2001; Sozinov et al., 2003). Lately CoNiAl has drawn considerable interest (Karaca et al., 2003; Morito et al., 2002). It needs to be emphasized that most of the experiments have utilized single-crystal specimens. The inelastic strain that can be generated in polycrystalline magnetic shape memory alloys is usually smaller (Cherechukin et al., 2001; Jeong et al., 2003; Murray et al., 1998; Ullakko et al., 2001; Wada et al., 2003). One effort aimed towards increasing the obtainable reorientation strain in polycrystals is based on the effect of favorable texture in these materials (cf. Marioni et al. (2002)).

Several models have been proposed in the literature that capture the variant reorientation process. The approach most commonly taken is the minimization of a free energy function characterizing the system to find equilibrium configurations for given magnetic, mechanical and thermal load conditions. The model presented by James and Wuttig (1998) is based on a *constrained theory of micromagnetics* (see also DeSimone and James (1997, 2002, 2003)). The terms contributing to the free energy in their model are the Zeeman energy, the magnetostatic energy and the elastic energy. The magnetization is assumed to be fixed to the magnetic easy axis of each martensitic variant because of high magnetic anisotropy. The microstructural deformations and the resulting macroscopic strain and magnetization response are predicted by detecting low-energy paths between initial and final configurations. They conclude that the typical strains observed in martensite, together with the typical easy axes observed in ferromagnetic materials lead to layered domain structures that are simultaneously mechanically and magnetically compatible.

O'Handley (1998) proposed a 2-D model in which two variants are separated by a single twin boundary and each variant itself consists of a single magnetic domain. The local magnetization is not necessarily constrained to the crystallographic easy axis. Depending on the magnitude of the magnetic anisotropy, either the magnetic anisotropy difference (low magnetic anisotropy case) or the Zeeman energy (high magnetic anisotropy case) are identified as the driving force for twin boundary motion. For the intermediate case a

parametric study is conducted showing the influence of varying elastic and magnetic anisotropy energies. All cases assume an initial variant distribution that implies a remnant magnetization.

Likhachev and Ullakko (2000a) presented a model which identifies the magnetic anisotropy energy difference in the two variant twinned-martensite microstructure as the main driving force for the reorientation process. The effect of magnetic domains is taken into account in an average sense through the incorporation of curve fitted magnetization data, corresponding to the magnetization along different crystallographic directions, into their model. They argue that, regardless of the physical nature of the driving force, twin boundary motion should be initiated at equivalent load levels. With this assumption experimentally obtained detwinning-under-stress data in addition to the magnetization data of magnetic shape memory alloy martensite can be used to predict the constitutive behavior associated with the variant reorientation process under the application of external magnetic fields.

Hirsinger and Lexcellent (2003b,a) introduced the outline of a non-equilibrium thermodynamics based model. The free energy contains chemical, mechanical, magnetic and thermal contributions. The magnetic term is given by the Zeeman energy. Two internal state variables, the martensitic variant volume fraction and the magnetic domain volume fraction, are introduced to represent the influence of the microstructure. The rate independent nature of their approach motivates the definition of driving forces for the twin boundary motion and the domain wall motion.

Glavatska et al. (2003) proposed a constitutive model for the martensitic twin rearrangement based on a statistical approach, in which the magnetic-field-induced strains are related to the relaxation of the internal stresses in martensite due to magnetoelastic interactions. It should be mentioned that several other groups have contributed to the literature on modeling of MSMAs, which can not all be mentioned in this brief overview. A more detailed review of the research on the modeling of MSMAs has recently been published by Kiang and Tong (2005)

It has previously been pointed out that most of the models found in the literature are based on the determination of equilibrium configurations through the minimization of a free energy function. However, in applications related to the design of structures with active materials, magneto-mechanical paths associated with the evolution of microstructure need to be modeled accounting for path dependence and hysteretic effects accompanying the magnetic shape memory effect. The approach taken in the present work is based on the evolution of thermodynamic states as governed by postulates concerning the dissipation of energy in such processes compatible with the second law of thermodynamics. The thermodynamic state of the material, characterized by a specific choice of independent state variables, is therefore not only determined by the current values of these state variables, but also by their history, accounted for by appropriate internal state variables.

A general approach to phenomenological modeling of the loading history dependent constitutive response of materials undergoing phase transformation, detwinning, or variant reorientation has widely been utilized in the literature on conventional shape memory alloys (Tanaka, 1986; Liang and Rogers, 1990; Boyd and Lagoudas, 1996; Lagoudas et al., 1996; Lubliner and Auricchio, 1996; Brinson and Huang, 1996; Bekker and Brinson, 1997; Bo and Lagoudas, 1999; Lagoudas and Bo, 1999; Govindjee and Hall, 2000). As mentioned, the austenite to martensite phase transformation in SMAs is induced by cooling or the application of mechanical forces. The independent state variables in this case are therefore usually chosen to be temperature and stress. In phenomenological constitutive modeling the system can be characterized by a macroscopic free energy expression which is a function of these independent state variables. A common approach of incorporating path dependence and dissipation is through the introduction of internal state variables (Coleman and Gurtin, 1967), whose evolution then accounts for the loading history dependence of the material behavior. Motivated by the crystallographic microstructure of martensite, a common choice for an internal state variable is the martensitic volume fraction. Constitutive equations, which relate the dependent state variables to the independent ones, follow directly from applying the well-known Coleman and Noll (1963) procedure commonly used in phenomenological modeling. The dependent state variables, such as the strain or entropy, are themselves also functions of the internal state variables through the constitutive relations and depend therefore on the loading history. The lack of apparent intrinsic time scales (diffusionless, thermoelastic phase transformation) makes the shape memory effect subject to rate independent modeling. This approach lends itself to the introduction of transformation functions, similar to yield functions of rate-independent plasticity models, which governs the onset and termination of the phase transformation (Qidwai and Lagoudas, 2000a). A transformation hardening function accounts for the interactions of different phases during the transformation process, which influence the activation of the phase transformation. The evolution of transformation

strain is related to the evolution of the martensitic volume fraction and its direction is given by a postulated transformation tensor (Boyd and Lagoudas, 1996).

The variant reorientation process in magnetic shape memory alloys is, from a modeling standpoint, also similar to the detwinning (i. e. self-accommodated to detwinned martensite) and reorientation (i. e. variation in the selection of martensitic variants under changes in the stress state) phenomena that are observed in conventional shape memory alloys (Bekker and Brinson, 1997; Leclercq and Lexcellent, 1996; Shu et al., 1997).

In order to apply the discussed approach of rate-independent phenomenological constitutive modeling to MSMAs, in addition to stress and temperature, in the present work an additional state variable, the magnetic field strength, is introduced in the expression of the free energy. This modeling approach has previously been discussed in (Kiefer and Lagoudas, 2004). A martensitic variant volume fraction and a magnetic domain volume fraction are identified as appropriate internal state variables. This choice is physically directly motivated by changes in the internal crystallographic and magnetic microstructure of the material which provide the mechanisms causing the macroscopically observable behavior. The thermodynamic framework is generalized to include magnetic field variables as well as magnetic energy terms. The derivation of constitutive equations for the dependent state variables entropy, strain and magnetization follows the same general procedure (Coleman and Noll, 1963) as discussed above. A reorientation function takes the role of the aforementioned transformation function, and governs the start and finish of the reorientation process. A hardening function accounts for the influence of the evolution of the martensitic variant volume fraction on the variation of critical field values for the reorientation process activation. The reorientation function, in combination with the incorporated hardening behavior, is physically interpreted based on a phase diagram in magnetic field vs. stress space. The evolution of the magnetic domain volume fraction is incorporated into the constitutive model in an analogous manner, by introducing a domain wall motion function, associated activation conditions and a corresponding hardening function.

The structure of the paper is as follows. The variant reorientation process is investigated in detail in Section 2, to promote a better understanding of the physical phenomena underlying the ferromagnetic shape memory effect. The observations made there are to be regarded as a physical motivation for the constitutive modeling approach which is pursued in this paper. Section 2.1 discusses the constitutive response in terms of macroscopic straining and the correlated magnetization of a MSMA single crystal under the application of magnetic fields and its connection to the crystallographic rearrangement of the martensitic variants. Section 2.2 takes a closer look at the magnetization of the martensitic phase in magnetic shape memory alloys. The magnetic anisotropy of the material is investigated by considering the magnetization of MSMAs along different crystallographic directions, when constrained to single variant configurations. A connection of the evolution of the magnetic microstructure to the macroscopic magnetization is established. Section 3 is concerned with the phenomenological modeling of magnetic shape memory alloys. First, Section 3.1 presents the generalized thermodynamic framework on which the modeling effort is based. The constitutive model capturing the magnetic shape memory effect is then derived in Section 3.2, based on the formulation of a specific free energy expression. To illustrate the validity and usefulness of the proposed model, an application to a specific example is conducted in Section 4. First, the governing equations are reduced for the special case in Section 4.1. Then, a procedure is introduced to obtain model parameters from experimental data in Section 4.2, which is directly applied to the considered case. The section ends with the presentation of numerical results on the strain vs. magnetic field response of a NiMnGa single crystal for varying biasing stress levels, in Section 4.3. The paper is concluded in Section 5 with a general discussion of the introduced constitutive model and an outlook on possible extensions of the presented approach in future work.

2 Influence of the Crystallographic and Magnetic Microstructure on the Macroscopic Constitutive Response of MSMAs

2.1 Induction of the macroscopic reorientation strain and the associated magnetization in MSMAs

The term magnetic shape memory effect (MSME) denotes the induction of large inelastic strains in the martensitic state of MSMAs under the application of external magnetic fields. For a rigorous understanding of the phenomena involved in causing this constitutive response, different length scales must be analyzed.

For instance, the observed macroscopic deformation of the material is connected to microstructural changes in the distribution of martensitic variants. In this paper the continuum scale, or macro-scale, is defined to generally span many magnetic domains and martensitic twin bands, which in turn span many crystallographic length scales. The macroscopic constitutive response is then related to the average material behavior, which is described by appropriate constitutive equations at a particular material point. At each material point, the average behavior is caused by mechanisms occurring on the micro-scale, which is the length scale of microstructural features such as magnetic domains, domain walls, martensitic variants, martensitic twins and twin boundaries.

In the magnetic shape memory alloy NiMnGa, the crystallographic structure of the low temperature martensite exhibits tetragonal symmetry. Figure 1 depicts the three possible tetragonal variants and introduces the nomenclature followed in this paper.[1] The undeformed austenite has cube edges of length a_0, whereas a and c refer to the long and short edges of the tetragonal unit cell associated with each martensitic variant, respectively. Typical lattice parameters for MSMAs with tetragonal martensite have for example been reported in Webster et al. (1984); Zasimchuk et al. (1990); Likhachev and Ullakko (2000b) for NiMnGa and in Cui et al. (2004) for FePd. Note that each of the martensitic variants are magnetized along a preferred crystallographic direction, named the magnetic easy axis, which in this case is aligned with the short edge c of the tetragonal unit cell, where it must be understood that the magnetization of a single unit cell is an idealized concept. The magnetization can be oriented in either the positive of negative easy axis direction. With this configuration of orthogonal preferred directions of magnetization, it is evident that the application of an external magnetic field can be used to favor selected variants over others, since an alignment of the magnetization and the magnetic field inside a magnetic material is energetically desirable. In the context of MSMA this process is referred to as the magnetic field-induced reorientation of martensitic variants, which is the microstructural mechanism causing the macroscopic magnetic shape memory effect.

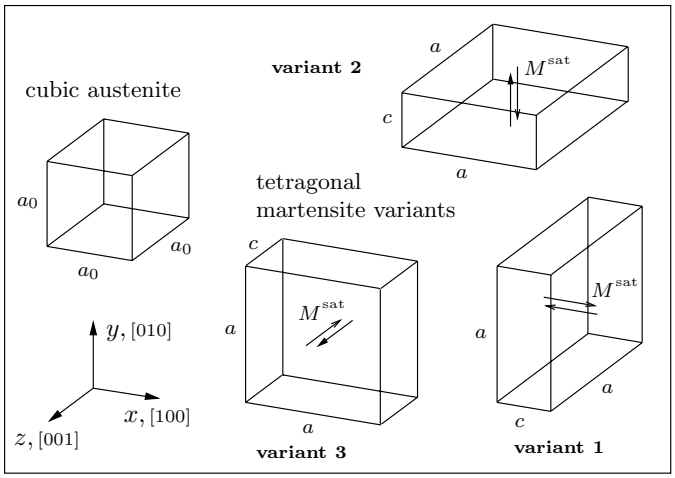

Figure 1: Crystal structure of the austenitic phase and the tetragonal martensite variants in NiMnGa. Arrows indicate the possible orientations of the saturation magnetization M^{sat} within each variant.

An experiment in which the strain vs. applied magnetic field response is measured has been reported by Tickle and James (1999); Tickle et al. (1999); Tickle (2000). A schematic illustration of the phenomena observed in this experiment is shown in Figure 2. Initially, the MSMA material is cooled under the application of a constant stress, thereby inducing the austenite to martenstite phase transformation. The applied compressive axial stress produces a single variant configuration of detwinned martensite, representing a clearly defined initial microstructure, which proves to be advantageous for the measuring of reorientation strains. The observed total strain consists of an elastic part, a transformation strain associated with the martensitic phase transformation, and the reorientation strain. The transformation strain is considered a constant quantity for the reorientation process, known from strain measurements during cooling from the austenitic reference state. Since completely detwinned martensite is produced in the phase transformation

[1] To be precise, the austenite in Ni_2MnGa is of $L2_1$ Heusler type structure, which is based on a fcc lattice. The martensite phase exhibits a bct structure, where the unit cell is rotated by 45° against the austenite lattice (cf. Murray et al. (2000b)). However, in most of the literature the more convenient description of the martensite structure depicted here has been adopted.

induced by cooling under applied stress, no additional detwinning of self-accommodated martensite occurs under the application of magnetic fields. Note that the stress is kept constant throughout the experiment, within a range whose lower bound is given by the minimum stress σ^{sv} necessary to ensure a detwinned single variant martensite configuration, and whose upper bound is the blocking stress σ^{b}. Above the blocking stress σ^{b} the magnetic shape memory effect caused by martensitic variant reorientation is completely suppressed (cf. Tickle and James, 1999).

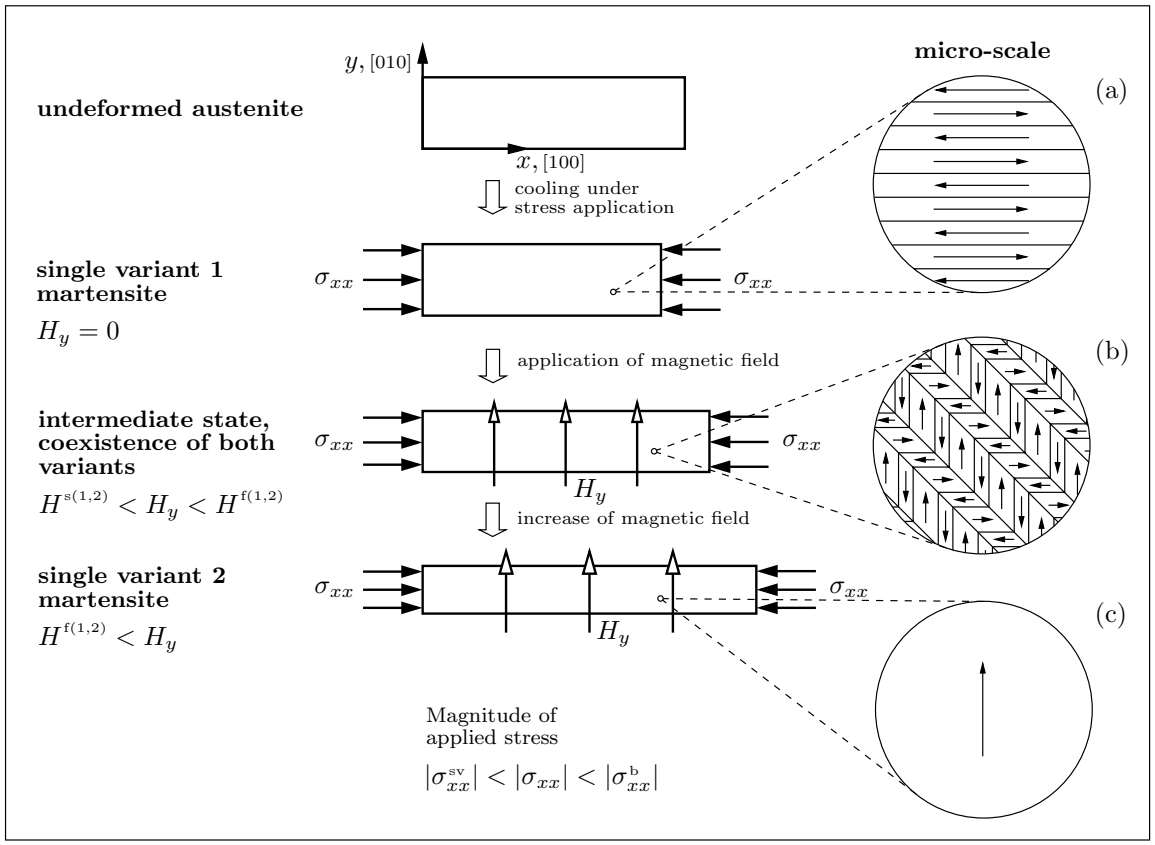

Figure 2: Schematic of several configurations of a NiMnGa single crystal specimen, corresponding to increasing applied magnetic field levels, as observed in an experiment devised to measure the strain vs. magnetic field response of NiMnGa under a constant compressive mechanical load (Tickle and James, 1999; Tickle, 2000). Additionally, Schematics (a)–(c) depict the respective magnetic and crystallographic microstructural arrangements of martensitic variants and magnetic domains.

For the martensitic variant 1 state an idealized schematic of the crystallographic and magnetic microstructure, at a generic material point, is shown in Schematic (a) at the right hand side of Figure 2. For this initial single variant state the micro-scale view depicts several magnetic domains. Magnetic domains are regions in which the magnetization is locally homogeneous and that are separated by magnetic domain walls, narrow regions in which the magnetization is rotated to accommodate the magnetization directions of neighboring domains (Kittel, 1949; Cullity, 1972; Spaldin, 2003). On the considered scale domain walls are essentially assumed to have zero thickness and in the schematic they are indicated by horizontal lines. Due to the considered tetragonal symmetry of martensite, the magnetization vectors are oriented along the horizontal [100]-direction, the easy axis of variant 1, and point in either the positive or negative coordinate direction, depending on the domain. Since there is no external magnetic field applied in this initial configuration, the domain arrangement yields a vanishing macroscopic magnetization. The magnetic energy terms whose competition governs the formation and size of magnetic domains and domain walls and the importance of the evolution of the magnetic microstructure with regards to the MSME are discussed in Section 2.2 in more detail.

The subsequent application of a transverse magnetic field H_y, above a critical threshold value, induces the nucleation of variant 2. The favored variant 2, then grows at the expense of variant 1 with increased H_y, resulting in the axial reorientation strain. The reorientation strain develops in this configuration, during the magnetic field-driven variant reorientation, because the long edge a of variant 2 replaces the short edge c of variant 1 along the [100] direction, thereby leading to an extension in that direction and contractions in the perpendicular directions. The evolution of the martensitic variant arrangement is quantified by considering the changes in variant volume fractions. Typical strain-magnetic field response curves, as measured in the described experiment, are qualitatively presented in Figure 3, for several increasing compressive stress levels. For an exemplary hysteresis loop this schematic introduces the notation for the threshold values $H^{\mathrm{s}(1,2)}$ and $H^{\mathrm{f}(1,2)}$ associated with the forward (variant 1 $\rightarrow$ variant 2), as well as $H^{\mathrm{s}(2,1)}$ and $H^{\mathrm{f}(2,1)}$ for the reverse (variant 2 $\rightarrow$ variant 1) reorientation process. The symbols s and f denoted the start and finish of the respective process, respectively.

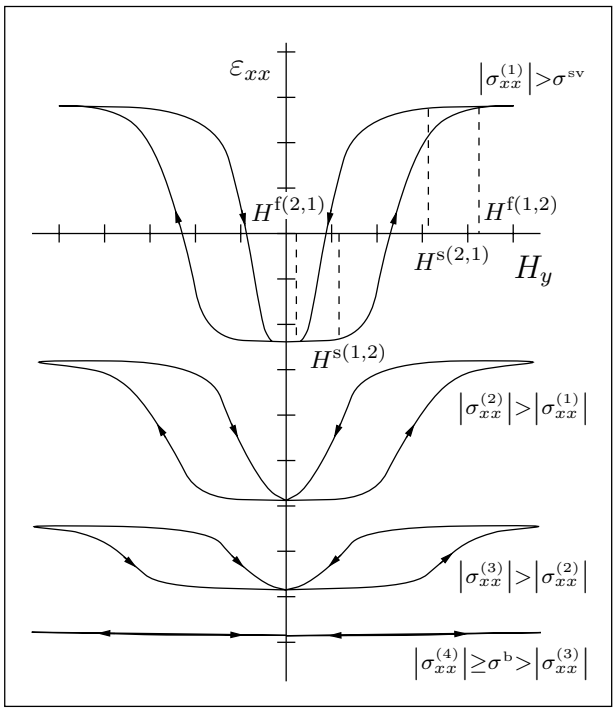

Figure 3: Schematic strain vs. magnetic field response of a MSMA single crystal for different axial bias stress levels.

As discussed, the macroscopic strain response shown in Figure 3 is caused by magnetic field-induced evolution of the magnetic and crystallographic microstructure. The microstructural arrangement for a generic intermediate applied magnetic field level $H^{\mathrm{s}(1,2)} < H_y < H^{\mathrm{f}(1,2)}$ is depicted in Schematic (b) of Figure 2. Again, horizontal and vertical lines indicate 180° magnetic domain walls, whereas slanted lines indicate twin boundaries, which also happen to coincide with 90° domain walls. In such a state, both variants coexist and form a twinned configuration. Two types of magnetic domains are present in each twin band. Note also that within each variant the magnetic domains in general have different volume fractions, yielding a non-zero macroscopic magnetization. The specimen is thereby magnetized in the process of applying the external magnetic field, simultaneously to the induction of the macroscopic reorientation strain. It must be emphasized at this point that the microstructures shown in Schematics 2(a),(b) are simplified in that they do not illustrate the local rotation of magnetization vectors, which generally also occurs in the magnetization process of MSMA. The influence of magnetization rotation within martensitic variants will be discussed in the following section.

Considering again Schematic 2(a), note that further increase of the magnetic field completely eliminates variant 1 at the threshold value of $H^{\mathrm{f}(1,2)}$, and for the resulting single variant 2 configuration the maximum reorientation strain is observed. Raising the magnetic field level above $H^{\mathrm{f}(1,2)}$ at which the reorientation process is complete, does not result in further straining of the material. The application of an external

magnetic field causes the simultaneous evolution of the magnetic domain structure such that for a large applied magnetic field the specimen consists of a single magnetic domain.

Quantitative experimental data corresponding to the qualitative macroscopic material response shown in Figure 3 have been published by Tickle et al. (1999); Tickle (2000). Note that the observed strain response is nonlinear and hysteretic, indicating dissipative effects associated with motion of twin boundaries. The strain axis intercepts of the hysteresis loops are related to the amount of compressive elastic strain and the transformation strain, since the undeformed austenite is taken to be the reference configuration. It should be observed that the maximum reorientation strain, as well as the size and shape of the hysteresis loops depend on the applied stress. The application of magnetic fields in the opposite direction produces the same hysteretic strain response. It must be pointed out the depicted curves represent an idealization of experimental observations, that captures most of the essential elements in the constitutive response of MSMA. Specifically, the response has been idealized in that it usually is nonsymmetric with respect to the positive and negative magnetic field cycle for some stress levels. Experimentally one actually observes a first cycle effect, because the maximum attainable strain in the first cycle is different from that of subsequent cycles (Karaman, 2004). If, for example, a positive magnetic field cycle is applied first and then followed up by a cycle of negative magnetic field application, the maximum reorientation strain value is observed to be smaller in the latter cycle. The maximum value for the reorientation strain essentially saturates within a first full cycle (one positive hysteresis loop and one negative hysteresis loop), so that it does not change for subsequent cycles, in which the strain response is then symmetric with respect to the strain axis. The curves schematically shown in Figure 3 represent stable hysteresis loops observed after a first complete cycle. The proposed model will be restricted to capturing only the characteristics of such stable hysteresis loops.

The next subsection deals with magnetic microstructures and the process of magnetizing a MSMA. Ultimately, it is the combination of the evolution of the martensitic variant and magnetic domain structure which provides the internal mechanisms that cause the macroscopic straining and magnetization of the material, and thus the magnetic shape memory effect. A detailed understanding of the mechanisms involved is essential for the modeling of the constitutive behavior.

2.2 Evolution of the magnetic microstructure in the magnetization of MSMAs

It has been indicated in Section 2.1, that the evolution of the reorientation strain is directly related to the magnetization of the MSMA material, since the reorientation process is driven by the magnetic field-controlled selection of martensitic variants. The evolution of the magnetic domain structure has qualitatively been described in Schematics (a)–(c) of Figure 2. However, these illustrations are based on certain assumptions concerning the magnetic properties of the considered material, which we proceed to investigate.

In general, the process of magnetizing a MSMA specimen involves several mechanisms which help to align the macroscopic magnetization with the external magnetic field. These include the nucleation and redistribution of martensitic variants, the magnetic domain wall motion and the rotation of the magnetization away from the preferred magnetic axis. In order to understand the influence of each of the mentioned mechanisms it is helpful to consider a thought experiment in which these effects can partially be separated. If the reorientation of martensitic variants in a MSMA single crystal is completely suppressed by the application of a stress above the blocking stress, then a change in the magnetization of the material by means of the nucleation of other more favorable variants is inhibited. The magnetization process of the MSMA in this case is comparable to that of regular ferromagnetic materials. Readers familiar with ferromagnetic materials will find the concepts introduced in the next few paragraphs basic, but they are included to ensure that all of the mechanisms involved in the magnetization of MSMAs are well understood before the details of the constitutive model are introduced.

Figure 4 shows a sketch of the initial single variant 1 configuration, which corresponds to that of Figure 2, except for the elevated stress level. Note that the phenomena that occur at stress levels above σ^{b} are not restricted to this specific biasing stress regime. They occur at all possible stress levels. However, the analysis of the influence of different mechanisms is greatly facilitated if the magnetization process is considered without the possibility of variant reorientation. Next to the macroscopic view of the specimen, Figure 4 also depicts schematics of the micro-scale and the crystallographic scale. The crystallographic scale is shown simply to indicate the fact that magnetic domains generally span many unit cells.

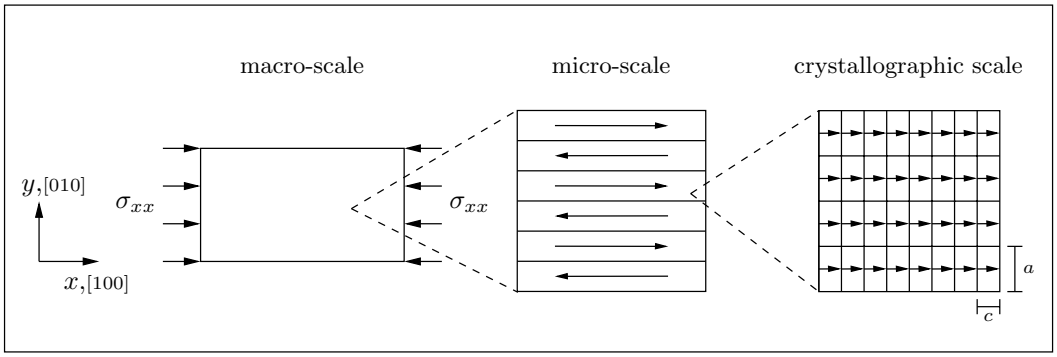

Figure 4: A schematic of the initial single variant 1 martensite state. The variant reorientation is suppressed by an axial compressive stress higher than the blocking stress. Also shown, schematics of the corresponding microscopic scale and the crystallographic scale.

Before analyzing the magnetization of a MSMA single crystal in the specific configuration presented in Figure 4, let us discuss the physical phenomena related to the formation of magnetic domains, and the magnetization of ferromagnetic materials in general, in more detail. From experimental observations it is evident that the application of external magnetic fields along different crystallographic directions is generally associated with varying energetic expense, which gives rise to the *magnetocrystalline anisotropy energy*. The direction along which the least amount of energy is required to magnetize the material is therefore termed the magnetic easy axis, and, correspondingly, the hard axis is the direction for which the most energy is expended. This anisotropic behavior of magnetic materials can be explained by the fact that varying mechanisms are activated in the magnetization along different crystallographic directions. To understand these mechanisms it is necessary to consider competing energy terms that play an important role in the formation and redistribution of magnetic domains. The *exchange energy* is based on quantum mechanical effects and acts to align neighboring magnetic dipole moments parallel to each other. It supports the formation of single domain configurations, which cause the material to be magnetized macroscopically. The thereby generated magnetostatic field, to which the magnetic body itself is subjected, tends to demagnetize it (Cullity, 1972). Associated with the built-up of this demagnetization field is the *magnetostatic energy*. To reduce this energy, multiple domains or closure domains are formed, which decrease the macroscopic magnetization and thereby the magnetostatic field outside the material body. The *Zeeman energy* is the main driving force in the redistribution of magnetic domains. It can be interpreted as the potential energy associated with the interaction between the magnetization of the material and an applied magnetic field. The magnetic domain structure is formed and evolves such that an alignment of the magnetization and the magnetic field is achieved.

The qualitative knowledge of the energy terms involved in the formation and evolution of magnetic domains is useful in the analysis of the macroscopic magnetization of the considered MSMA. Let us investigate in this thought experiment the magnetization of the single variant martensitic specimen (Figure 4) along two specific crystallographic directions, namely the compression axis and the axis perpendicular to it.

- **Magnetization along the compression axis (easy axis)**: Figure 5 schematically shows the magnetic domain distribution at different applied field levels for the magnetization of the MSMA specimen along the [100]-direction. The starting point in Figure 5 (left box) is the same microstructural view of the compressed single variant specimen as was presented in Figure 4 (middle box). Note that since the external field is applied in the [100]-direction, the magnetization to saturation can be realized by mostly reversible 180° domain wall motion, requiring a low amount of energy, making this direction the easy axis of magnetization.

  Note also, that no ordinary magnetostrictive change in dimensions is associated with the mechanism of 180° domain wall motion. Ordinary magnetostriction thereby refers to the deformation of the MSMA under the application of magnetic fields, which is not associated with the reorientation of martensitic variants. Even though magnetostrictive strains are usually at least one order of magnitude smaller than the reorientation strain in MSMA, changes in the elastic energy due to these deformations can potentially influence the overall constitutive response.

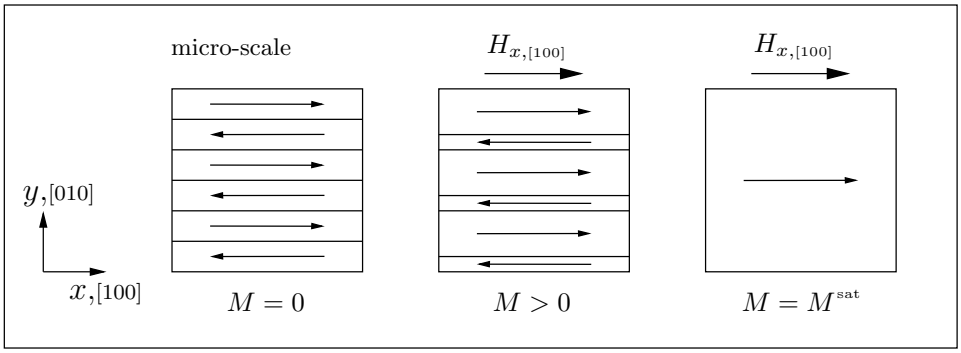

Figure 5: Magnetization of the single variant specimen along the compression axis (easy axis).

The change in the macroscopic magnetization by means of magnetic domain wall motion can be observed in the previously presented configuration for intermediate field values (Figure 2). Note that in Schematic 2a the favored domains are of greater volume fraction than their unfavored counterparts, which are continuously reduced for increasing magnetic fields. It has been argued in the literature that unfavorable magnetic domains are eliminated in MSMAs at relatively low magnetic field levels at the very beginning of the reorientation process. This point will be discussed in more detail in Section 4.1.

- **Magnetization along the perpendicular axis (hard axis)**: As indicated in Figure 6, no domain wall motion mechanism is available to accommodate the magnetization along the [010]-direction. The magnetization in both domains must be rotated away from the easy axis. The rotation of the magnetization within a martensitic variant requires work against the magnetocrystalline anisotropy energy. The amount of energy expended in activating this mechanism is higher than that associated with domain wall motion. The [010]-direction is therefore the hard axis for this material. The magnetization of the MSMA specimen along directions in between [100] and [010], requires an intermediate amount of energy. Unlike the motion of 180° domain walls, the rotation of the magnetization inside of the martensitic variant is coupled with ordinary magnetostriction.

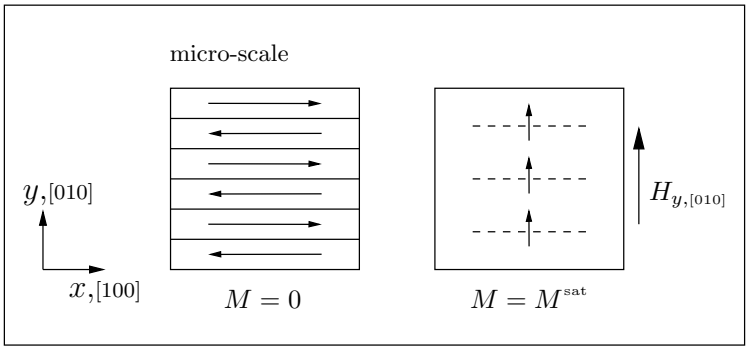

Figure 6: Magnetization of the single variant specimen perpendicular to the compression axis (hard axis).

Figure 7 shows the corresponding qualitative magnetization curves for the easy [100] and the hard [010]-directions. The coordinate axes are normalized by the saturation magnetization M^{sat} and an arbitrary maximum applied field value H^{max}, respectively. The magnetization curves in Figure 7 are understood in the context of the mechanisms presented in Figures 5 and 6. Recall that the mechanism of accommodation in the magnetic microstructure is the domain wall motion, in the easy axis case, and rotation of the magnetization, in the case of the hard axis. Experiments of this nature have in fact been conducted for NiMnGa and the results have been reported by Tickle and James (1999). Similar results have been published by Likhachev and Ullakko (2000a), Shield (2003) and Cui et al. (2004).

The analysis of the experimental results such as those qualitatively presented in Figure 7 is of great importance for the development of a phenomenological constitutive model which captures the macroscopic

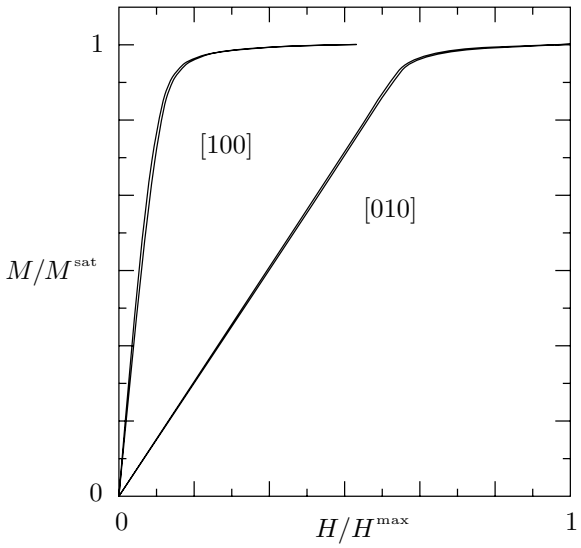

Figure 7: Qualitative magnetization curves of the single variant MSMA specimen magnetized along the compression and perpendicular axes. For quantitative experimental results cf. Tickle and James (1999).

strain response associated with the magnetic shape memory effect as presented in Figures 2 and 3 of Section 2.1. It has been shown how, in the induction of the reorientation strain, both the evolution of the martensitic variant distribution as well as the magnetic microstructure play an essential role. To model the magnetization and the associated deformation of the MSMA, the mechanisms of domain wall motion, magnetization rotation as well as the nucleation and reorientation of martensitic variants must all be taken into account.

We have thus briefly presented the microstructural mechanisms which cause the macroscopic strain response and the corresponding magnetization of the MSMA under the application of external magnetic fields. This information motivates the incorporation of the evolution of the crystallographic and magnetic microstructure into the phenomenological constitutive model, which in this work is realized through the introduction of appropriate internal state variables. First, however, a general thermo-magneto-mechanical framework must be established, which is done in the following section.

3 Phenomenological Modeling of the Magnetic Shape Memory Alloy Constitutive Behavior

3.1 Thermodynamic framework for the phenomenological modeling of MSMAs

Magnetic shape memory alloys can be considered as continua that deform under mechanical and magnetic forces. All state variables are defined at a generic material point of the continuum. The thermodynamic state of the material body can be characterized by the Gibbs free energy function G, which depends on the independent state variables temperature T, the Cauchy stress tensor $\boldsymbol{\sigma}$ and the magnetic field strength $\mathbf{H}$ as well as a set of internal state variables. In addition to the inelastic reorientation strain $\boldsymbol{\varepsilon}^{\mathrm{r}}$, the internal state variables are given by a generic set $\boldsymbol{\zeta}$. Specific choices for those variables are going to be made in Section 3.2.1, based on physical motivation by the crystallographic and magnetic microstructure of MSMAs. The method of incorporating dissipative effects, and thereby loading history dependence, into the free energy expression through internal state variables was originally proposed by Coleman and Gurtin (1967).

The Gibbs free energy is related to the internal energy $u = \hat{u}(s, \boldsymbol{\varepsilon}^{\mathrm{te}}, \mathbf{M}, \boldsymbol{\varepsilon}^{\mathrm{r}}, \boldsymbol{\zeta})$ through the Legendre transformation

$$G = \hat{G}(T, \boldsymbol{\sigma}, \mathbf{H}, \boldsymbol{\varepsilon}^{\mathrm{r}}, \boldsymbol{\zeta}) = u - sT - \frac{1}{\rho}\,\boldsymbol{\sigma}\!:\!\boldsymbol{\varepsilon}^{\mathrm{te}} - \frac{\mu_0}{\rho}\,\mathbf{H}\cdot\mathbf{M}\,, \tag{1}$$

where s is the specific entropy, ρ is the mass density, $\boldsymbol{\varepsilon}^{\mathrm{te}}$ the thermoelastic strain tensor, μ_0 the permeability of free space and $\mathbf{M}$ the magnetization.

In the context of the magnetic shape memory effect that has been introduced in Section 2.1, different components of the total strain need to be distinguished. Deformations corresponding to different stages of the loading cycle are schematically indicated in Figure 2 and corresponding strain curves have been presented in Figure 3. It has implicitly been assumed in equation (1) that for a small strain approximation the additive decomposition

$$\boldsymbol{\varepsilon} = \boldsymbol{\varepsilon}^{\mathrm{te}} + \boldsymbol{\varepsilon}^{\mathrm{r}} + \bar{\boldsymbol{\varepsilon}}^{\mathrm{tr}} \,, \tag{2}$$

is appropriate. Here, the reference state for the measured strain is the undeformed austenite. The thermoelastic part of the total strain tensor is reversible and the irreversible part consists of the reorientation strain $\boldsymbol{\varepsilon}^{\mathrm{r}}$ and the transformation strain $\bar{\boldsymbol{\varepsilon}}^{\mathrm{tr}}$. The transformation strain occurs when the austenitic material is cooled below the martensitic finish temperature under the application of stress and the phase transformation produces detwinned martensite. The bar indicates that the quantity is constant (i. e. $\dot{\bar{\boldsymbol{\varepsilon}}}^{\mathrm{tr}} = 0$) throughout the reorientation process, as the material remains entirely in the martensitic state. It must further be remarked that the thermo-magneto-mechanical framework introduced in this paper is in general not limited to a small strain formulation. Finite strain models have been presented in the literature in the context of conventional SMAs, which employ the same thermo-mechanical framework (cf. Qidwai and Lagoudas, 2000b).

The conservation of energy is expressed in the *first law of thermodynamics*, which in the local form is given by (Malvern, 1969)

$$\rho \dot{u} = \boldsymbol{\sigma} : \dot{\boldsymbol{\varepsilon}} + \mu_0 \mathbf{H} \cdot \dot{\mathbf{M}} - \operatorname{div} \mathbf{q} + \rho r^{\mathrm{h}} \,, \tag{3}$$

with $\mathbf{q}$ denoting the heat flux vector and r^{h} a heat source. The additional contribution of the magnetic field to the rate of change of the internal energy of a material body, represented by the term $\mu_0 \mathbf{H} \cdot \dot{\mathbf{M}}$, has been discussed by several authors (Truesdell and Toupin, 1960; Tiersten, 1964; Brown, 1966; Penfield Jr. and Haus, 1967; Pao and Hutter, 1975; Hutter and van de Ven, 1978; Eringen and Maugin, 1990a,b; Maugin, 1999).

A limitation on the direction in which a thermodynamic process can be carried out in a physical system is given by the *second law of thermodynamics*, which can be formulated in terms of the internal entropy production rate γ (Malvern, 1969) as

$$\gamma := \dot{s} - \frac{r^{\mathrm{h}}}{T} + \frac{1}{\rho T} \operatorname{div} \mathbf{q} - \frac{1}{\rho T^2} \, \mathbf{q} \cdot \nabla T \geq 0 \,. \tag{4}$$

Following the well-known procedure of Coleman and Noll (1963), in utilizing equations (1), (3) and (4), one derives the *Clausius-Duhem inequality*, which is a combination of the first and second law of thermodynamics as presented in the local form of (3) and (4), as

$$\begin{aligned} &- \rho \left(s + \frac{\partial G}{\partial T} \right) \dot{T} - \left(\boldsymbol{\varepsilon}^{\mathrm{te}} + \rho \frac{\partial G}{\partial \boldsymbol{\sigma}} \right) : \dot{\boldsymbol{\sigma}} - \left(\mu_0 \mathbf{M} + \rho \frac{\partial G}{\partial \mathbf{H}} \right) \dot{\mathbf{H}} \\ &+ \left(\boldsymbol{\sigma} - \rho \frac{\partial G}{\partial \boldsymbol{\varepsilon}^{\mathrm{r}}} \right) : \dot{\boldsymbol{\varepsilon}}^{\mathrm{r}} - \rho \frac{\partial G}{\partial \boldsymbol{\zeta}} \cdot \dot{\boldsymbol{\zeta}} - \frac{1}{T} \, \mathbf{q} \cdot \nabla T \;\geq\; 0 \,. \end{aligned} \tag{5}$$

Note that the rates $\dot{T}$, $\dot{\boldsymbol{\sigma}}$ and $\dot{\mathbf{H}}$ appear linearly in equation (5). Through the constitutive assumption (1), their parenthesized coefficients only depend on the set of state variables $(T, \boldsymbol{\sigma}, \mathbf{H}, \boldsymbol{\varepsilon}^{\mathrm{r}}, \boldsymbol{\zeta})$, not their rates. Therefore, in order for the inequality to hold for arbitrary processes, these coefficients must vanish, which leads to the constitutive relations

$$s = -\frac{\partial G}{\partial T} \,; \qquad \boldsymbol{\varepsilon}^{\mathrm{te}} = -\rho \frac{\partial G}{\partial \boldsymbol{\sigma}} \,; \qquad \mu_0 \mathbf{M} = -\rho \frac{\partial G}{\partial \mathbf{H}} \,. \tag{6}$$

The coefficients of $\dot{\boldsymbol{\varepsilon}}^{\mathrm{r}}$ and $\dot{\boldsymbol{\zeta}}$ in the inequality (5) can, however, in general depend on the rates of the internal state variables and therefore need not vanish. This dependence can thereby not be arbitrary, but is governed by the reduced Clausius-Duhem inequality

$$\boldsymbol{\sigma}^{\mathrm{eff}} : \dot{\boldsymbol{\varepsilon}}^{\mathrm{r}} - \rho \frac{\partial G}{\partial \boldsymbol{\zeta}} \cdot \dot{\boldsymbol{\zeta}} - \frac{1}{T} \, \mathbf{q} \cdot \nabla T \geq 0 \,, \tag{7}$$

where the definition of an effective stress tensor $\boldsymbol{\sigma}^{\mathrm{eff}} := \boldsymbol{\sigma} - \rho \frac{\partial G}{\partial \boldsymbol{\varepsilon}^{\mathrm{r}}}$ has been introduced.

3.2 Derivation of a model accounting for the variant reorientation process in MSMAs

The thermo-magneto-mechanical framework has now been established on which a phenomenological model can be built. The approach taken here is to propose a specific form of the free energy function (1) whose terms are motivated by the analysis of the development of the reorientation strain and the magnetization associated with the magnetic shape memory effect, as they have been discussed in Section 2. The influence of the changing crystallographic and magnetic microstructure is incorporated through the introduction of suitable internal state variables, which account for the dissipative effects associated with the twin boundary and domain wall motion in the evolution of the inelastic reorientation strain. Additional internal state variables are introduced to describe changes in the free energy caused by the local rotation of the magnetization away from magnetic easy axes, which can be considered as a reversible process and thus the latter phenomenon does not contribute to the entropy production. According to the constitutive relations (6), the expressions for the dependent state variables entropy s, thermoelastic strain $\boldsymbol{\varepsilon}^{\mathrm{te}}$ and magnetization $\mathbf{M}$, follow directly from taking partial derivatives of the specific Gibbs free energy function with respect to the independent state variables temperature T, mechanical stress $\boldsymbol{\sigma}$ and magnetic field strength $\mathbf{H}$. Through the derived constitutive relations, the dependent state variables also depend on the internal state variables, whose evolution thereby accounts for the loading history dependence of the material behavior.

Another possible approach that has been used in the modeling of shape memory materials is to explicitly account for micro-scale phenomena, such as the interaction of martensitic variants, and their influence on the macroscopic material behavior, which is determined by using appropriate averaging techniques (cf. Patoor et al., 1996). In the phenomenological approach taken here, the effective constitutive response at a material point and its variation with the evolution of the microstructure is represented by the evolution of the internal state variables and their coupling to the prescribed nature of the hardening behavior.

3.2.1 The choice of internal state variables

In order to motivate the introduction of specific internal state variables for the MSMA constitutive model we again consider the influence of the crystallographic and magnetic microstructure on the macroscopic constitutive response as it has been addressed qualitatively in Section 2. Recall that in the 2-D case, two martensitic variants, and two magnetic domain types coexist. To explain the nomenclature and the assumptions associated with the introduction of these variables Figure 8 takes a closer look at the microstructure that has previously been shown in Figure 2, for a generic intermediate applied magnetic field level. Note that in this sketch the possibility of a rotation of the local magnetization away from the magnetic easy axes is included. Variant 1 (cf. Figure 1 for terminology) is magnetized along the x, [100]-direction, whereas variant 2 has its magnetic easy axis along the y, [010]-direction. The magnetic domains are defined by the orientation of the magnetization. Magnetic domain 1 refers to parts of the magnetic microstructure in which the magnetization, when aligned with the easy axis, is oriented in the negative direction of the respective coordinate axis, and in domain 2 it points in the opposite direction.

Motivated by this 2-D arrangement of the microstructure the scalar martensitic variant 2 volume fraction ξ and the magnetic domain 2 volume fraction α are introduced. Correspondingly, the volume fraction of variant 1 is $(1-\xi)$, and that of domain 1 is $(1-\alpha)$. As mentioned, the third internal variable is the reorientation strain $\boldsymbol{\varepsilon}^{\mathrm{r}}$, whose evolution contributes to the total strain and is later connected to the evolution of the martensitic variant volume fraction. To account for the local rotation of the magnetization vectors the angles θ_i, with $(-\frac{\pi}{2} \leq \theta_i \leq \frac{\pi}{2})$, are introduced as additional internal state variables, where the subscript i refers to one of the four sub-regions indicated in Figure 8. Each of these regions refers to one of the four possible combinations of martensitic variants and magnetic domains in the considered arrangement. Note that as indicated in Figure 8 the local magnetization vectors and their associated rotation angles are considered constant within each domain. Note that the rotations shown in the sketch do not necessarily correspond to realistic arrangement of magnetization vectors, but serve the purpose of illustrating the nomenclature. Compatibility of domains along a twin plane, which separates different variants, has also been assumed, meaning that the domain walls of neighboring twins meet on the twin boundary in a compatible manner.

For this microstructural configuration the four distinct magnetization directions that exist have the specific

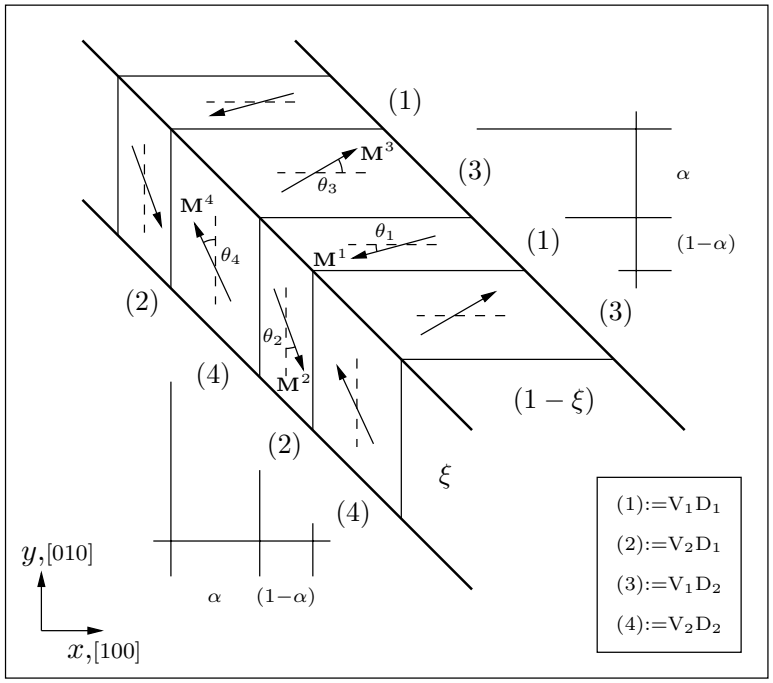

Figure 8: Coexistence of martensitic variants and magnetic domains at a twin boundary during the reorientation process. The angles θ_i represent the rotation of magnetization vectors (solid arrows) with respect to the magnetic easy axes along which they are oriented in their reference configurations (dashed arrows). The abbreviation $\mathrm{V}_1\mathrm{D}_2$, for example, stands for "variant 1, domain 2". The four distinct subdomains are numbered 1–4 to simplify the notation.

magnetization vectors

$$\begin{aligned}
&\mathbf{M}^1 := \mathbf{M}^{\mathrm{V_1D_1}} = -M^{\mathrm{sat}}\big(\cos(\theta_1)\,\mathbf{e}_x + \sin(\theta_1)\,\mathbf{e}_y\big)\ , \quad \mathbf{M}^2 := \mathbf{M}^{\mathrm{V_2D_1}} = M^{\mathrm{sat}}\big(\sin(\theta_2)\,\mathbf{e}_x - \cos(\theta_2)\,\mathbf{e}_y\big)\ , \\
&\mathbf{M}^3 := \mathbf{M}^{\mathrm{V_1D_2}} = M^{\mathrm{sat}}\big(\cos(\theta_3)\,\mathbf{e}_x + \sin(\theta_3)\,\mathbf{e}_y\big) \quad , \quad \mathbf{M}^4 := \mathbf{M}^{\mathrm{V_2D_2}} = M^{\mathrm{sat}}\big(-\sin(\theta_4)\,\mathbf{e}_x + \cos(\theta_4)\,\mathbf{e}_y\big)\ ,
\end{aligned} \tag{8}$$

which each contribute to the effective magnetization at a material point, such that

$$\mathbf{M} = (1-\xi)\Big[(1-\alpha)\mathbf{M}^1 + \alpha\mathbf{M}^3\Big] + \xi\Big[(1-\alpha)\mathbf{M}^2 + \alpha\mathbf{M}^4\Big]\ . \tag{9}$$

M^{sat} is the saturation magnetization and $\mathbf{e}_x, \mathbf{e}_y$ are unit vectors in the respective coordinate directions. If the magnetization vectors are assumed to be fixed to the respective magnetic easy axes (i. e. $\theta_i = 0$) this representation of the microstructure reduces to the formulation previously proposed in the literature by Hirsinger and Lexcellent (2003b).

3.2.2 Formulation of the specific Gibbs free energy

On the basis of the assumed microstructure and the resulting choice of internal state variables the Gibbs free energy is constructed as a weighted average between the contributions of each variant. In each step the deviation of the total free energy from the weighted average of the constituents is accounted for by an additional mixing term to account for the interactions of martensitic variants

$$\begin{aligned}
G &= \hat{G}(T, \boldsymbol{\sigma}, \mathbf{H}, \xi, \boldsymbol{\varepsilon}^{\mathrm{r}}, \alpha, \theta_j) \\
&= \xi G^{\mathrm{V_2}}(T, \boldsymbol{\sigma}, \mathbf{H}, \alpha, \theta_2, \theta_4) + (1-\xi) G^{\mathrm{V_1}}(T, \boldsymbol{\sigma}, \mathbf{H}, \alpha, \theta_1, \theta_3) + G^{\xi\text{-mix}}(\xi, \boldsymbol{\varepsilon}^{\mathrm{r}})\ ,
\end{aligned} \tag{10}$$

with $j = 1, \ldots, 4$.

The contribution of each martensitic variant $G^{\mathrm{V_i}}$, $(i=1,2)$ to the total Gibbs free energy (10) is proposed to be given by

$$G^{\mathrm{V_i}} = -\frac{1}{2\rho}\,\boldsymbol{\sigma}:\mathcal{S}^{\mathrm{V_i}}\boldsymbol{\sigma} + (1-\alpha)\left[-\frac{\mu_0}{\rho}\mathbf{M}^{\mathrm{V_iD_1}}\cdot\mathbf{H} + G^{\mathrm{an,V_iD_1}}\right] + \alpha\left[-\frac{\mu_0}{\rho}\mathbf{M}^{\mathrm{V_iD_2}}\cdot\mathbf{H} + G^{\mathrm{an,V_iD_2}}\right] + G^{\alpha\text{-mix}}(\alpha) + G_0(T)\;. \tag{11}$$

Here, $\mathcal{S}^{\mathrm{V_i}}$ denotes the elastic compliance tensor of variant i. The density does not differ in the two martensitic variants and the reorientation process is volume conserving.

Note that in (11) the macroscopic magnetization at a generic material point is constructed as a weighted average of the possible micro-scale magnetization directions that have been introduced in (8). The weighting factors are the respective magnetic domain volume fractions, a concept previously proposed by Hirsinger and Lexcellent (2003b,a). A mixing term $G^{\alpha\text{-mix}}$ accounts for the interaction of different magnetic domains. The scalar quantity G_0 is a reference state value of the Gibbs free energy, which includes the change due to the initial austenite to martensite phase transformation. If isothermal conditions are assumed for the reorientation process, G_0 is a constant.

The total Gibbs free energy must in general contain an elastic, a magnetic and a magnetoelastic part. The magnetoelastic contribution in the form of ordinary magnetostriction, however, is neglected since the associated strains are at least two orders of magnitude smaller in MSMAs than the strains caused by the variant rearrangement (Tickle and James, 1999). The elastic part is included in the total free energy functional (10), using (11), in the form of the elastic strain energy. The magnetic part contains both the magnetocrystalline anisotropy energy and the Zeeman energy terms, which have been identified as the magnetic driving forces for the variant reorientation and the associated magnetization process. These magnetic energy terms have previously been discussed in Section 2.2 in the context of magnetic domain formation. The exchange energy has been excluded on the considered scale cf. DeSimone (1993); Shield (2003)). The magnetostatic energy mentioned in Section 2.2 has not been included explicitly because of its dependence on the geometry of the considered material body. A continuum level constitutive behavior, which relates the independent state variables to the dependent ones at a particular material point, can by definition not include effects that dependent on the boundary of the modeled domain. It is understood, however, that the internal magnetic field at that material point may be different from the externally applied field due to the demagnetization effect which is influenced by the geometry. As mentioned, the magnetostatic energy is associated with the build-up of the demagnetizing field. The demagnetizing effect is taken into account when solving the magneto mechanical boundary value problem, i. e. the coupled set of Maxwell's equations, mechanical equilibrium equations and constitutive relations with appropriate boundary conditions, for the internal magnetic field acting at the considered point in the continuum with given external magnetic field, stress, temperature values and loading history.

Recall that the magnetocrystalline anisotropy energy G^{an} accounts for changes in the free energy due to the rotation of magnetization vectors within the magnetic domains. An explicit form of the anisotropy energy for *uniaxial symmetry*, which is an adequate assumption, is usually given in a series expansion as (cf. Kittel (1949); Kittel and Galt (1956); O'Handley (2000))[2]

$$G^{\mathrm{an}} = \sum_{n=0}^{N} K_n \sin^{2n}(\theta)\;. \tag{12}$$

In the literature on MSMA lower order symmetries, such as tetragonal symmetry (Cui et al., 2004), have also been considered. Experimental observations that corrections of the anisotropy coefficients due to stress anisotropy effects related to ordinary magnetostriction in the single variant state are small enough to be neglected (Tickle, 2000).

[2]This series expansion is valid for an unstrained crystal. However, because of the high magnetocrystalline anisotropy observed in MSMA materials, the influence of stress application on the anisotropy through ordinary magnetostriction is negligible, as was indicated by experiments performed by Tickle (2000).

The influence of the interaction of evolving martensitic variants or magnetic domains on the free energy, generically introduced in (10) by the mixing terms $G^{\xi\text{-mix}}$ and $G^{\alpha\text{-mix}}$, respectively, is assumed to be captured by hardening functions of the form

$$\begin{aligned} G^{\xi\text{-mix}} &= \frac{1}{\rho}\, f^{\xi}(\xi, \boldsymbol{\varepsilon}^{\mathrm{r}}) \,, \\ G^{\alpha\text{-mix}} &= \frac{1}{\rho}\, f^{\alpha}(\alpha) \,. \end{aligned} \tag{13}$$

By postulating a hardening function associated with the reorientation process, for example, the effective hardening behavior, which is due to micro-scale interactions of the different martensitic variants, is macroscopically taken into account in an average phenomenological sense. Specific forms of these functions are introduced in Section 4.1.

The combination of equations (10), (11) and (13) yields the explicit form of the total Gibbs free energy

$$\begin{aligned} G &= G(T, \boldsymbol{\sigma}, \mathbf{H}, \xi, \boldsymbol{\varepsilon}^{\mathrm{r}}, \alpha, \theta_j) \\ &= -\frac{1}{2\rho}\, \boldsymbol{\sigma} : \mathcal{S}\boldsymbol{\sigma} + \xi \Big[(1-\alpha) \Big[-\frac{\mu_0}{\rho} \mathbf{M}^2 \cdot \mathbf{H} + G^{\mathrm{an},2}(\theta_2) \Big] + \alpha \Big[-\frac{\mu_0}{\rho} \mathbf{M}^4 \cdot \mathbf{H} + G^{\mathrm{an},4}(\theta_4) \Big] \Big] \\ &\quad + (1-\xi) \Big[(1-\alpha) \Big[-\frac{\mu_0}{\rho} \mathbf{M}^1 \cdot \mathbf{H} + G^{\mathrm{an},1}(\theta_1) \Big] + \alpha \Big[-\frac{\mu_0}{\rho} \mathbf{M}^3 \cdot \mathbf{H} + G^{\mathrm{an},3}(\theta_3) \Big] \Big] \\ &\quad + \frac{1}{\rho}\, f^{\xi}(\xi, \boldsymbol{\varepsilon}^{\mathrm{r}}) + \frac{1}{\rho}\, f^{\alpha}(\alpha) + G_0(T) \,, \end{aligned} \tag{14}$$

where $\mathcal{S} := \mathcal{S}^{\mathrm{V}_1} + \xi \Delta\mathcal{S} = \mathcal{S}^{\mathrm{V}_1} + \xi(\mathcal{S}^{\mathrm{V}_2} - \mathcal{S}^{\mathrm{V}_1})$ is the effective compliance tensor. For isotropic cases, it has been shown by the use of micromechanical techniques, that this linear average for effective material properties is a good approximation (Boyd and Lagoudas, 1996; Bo and Lagoudas, 1999; Entchev and Lagoudas, 2001).

From the constitutive equations (6) specific relations then follow for the entropy, the thermoelastic strain and the magnetization

$$\begin{aligned} s &= -\frac{\partial G}{\partial T} = -\frac{\partial G_0}{\partial T} \,, \\ \boldsymbol{\varepsilon}^{\mathrm{te}} &= -\rho \frac{\partial G}{\partial \boldsymbol{\sigma}} = \mathcal{S}\boldsymbol{\sigma} \,, \\ \mathbf{M} &= -\frac{\rho}{\mu_0} \frac{\partial G}{\partial \mathbf{H}} = \xi \big[(1-\alpha)\mathbf{M}^2 + \alpha \mathbf{M}^4 \big] + (1-\xi) \big[(1-\alpha)\mathbf{M}^1 + \alpha \mathbf{M}^3 \big] \\ &= M^{\mathrm{sat}} \xi \Big[(1-\alpha) \big(\sin(\theta_2)\, \mathbf{e}_x - \cos(\theta_2)\, \mathbf{e}_y \big) + \alpha \big(-\sin(\theta_4)\, \mathbf{e}_x + \cos(\theta_4)\, \mathbf{e}_y \big) \Big] \\ &\quad + M^{\mathrm{sat}} (1-\xi) \Big[-(1-\alpha) \big(\cos(\theta_1)\, \mathbf{e}_x + \sin(\theta_1)\, \mathbf{e}_y \big) + \alpha \big(\cos(\theta_3)\, \mathbf{e}_x + \sin(\theta_3)\, \mathbf{e}_y \big) \Big] \,. \end{aligned} \tag{15}$$

Note that according to (15a) the entropy is only a function of temperature, and therefore must be constant throughout the reorientation process, if isothermal conditions are assumed. This means that the entropy changes due to dissipative effects must be balanced by suitable heat transfer to maintain a constant temperature.

By taking derivatives of the total free energy with respect to the internal state variables, i. e. the reorientation strain, the martensitic variant volume fraction and the magnetic domain volume fraction, the following thermodynamic driving forces are derived

$$
\begin{aligned}
\tilde{\boldsymbol{\pi}}^{\mathrm{r}} &:= \boldsymbol{\sigma} - \rho\frac{\partial G}{\partial \boldsymbol{\varepsilon}^{\mathrm{r}}} = \boldsymbol{\sigma}^{\mathrm{eff}} \,, \\
\tilde{\pi}^{\xi} &:= -\rho\frac{\partial G}{\partial \xi} = \frac{1}{2}\,\boldsymbol{\sigma}:\Delta\mathcal{S}\boldsymbol{\sigma} - \rho\Big[(1-\alpha)\Big[-\frac{\mu_0}{\rho}\mathbf{M}^2\cdot\mathbf{H} + G^{\mathrm{an},2}(\theta_2)\Big] + \alpha\Big[-\frac{\mu_0}{\rho}\mathbf{M}^4\cdot\mathbf{H} + G^{\mathrm{an},4}(\theta_4)\Big]\Big] \\
&\qquad + \rho\Big[(1-\alpha)\Big[-\frac{\mu_0}{\rho}\mathbf{M}^1\cdot\mathbf{H} + G^{\mathrm{an},1}(\theta_1)\Big] + \alpha\Big[-\frac{\mu_0}{\rho}\mathbf{M}^3\cdot\mathbf{H} + G^{\mathrm{an},3}(\theta_3)\Big]\Big] - \frac{\partial f^{\xi}}{\partial \xi} \,, \\
\pi^{\alpha} &:= -\rho\frac{\partial G}{\partial \alpha} = \rho\xi\Big[G^{\mathrm{an},2}(\theta_2) - G^{\mathrm{an},4}(\theta_4) + \frac{\mu_0}{\rho}\big(\mathbf{M}^4 - \mathbf{M}^2\big)\cdot\mathbf{H}\Big] \\
&\qquad + \rho(1-\xi)\Big[G^{\mathrm{an},1}(\theta_1) - G^{\mathrm{an},3}(\theta_3) + \frac{\mu_0}{\rho}\big(\mathbf{M}^3 - \mathbf{M}^1\big)\cdot\mathbf{H}\Big] - \frac{\partial f^{\alpha}}{\partial \alpha} \,, \\
\pi^{\theta_1} &:= -\rho\frac{\partial G}{\partial \theta_1} = -\rho(1-\xi)(1-\alpha)\Big[\frac{\mu_0 M^{\mathrm{sat}}}{\rho}\Big[-\sin(\theta_1)H_x + \cos(\theta_1)H_y\Big] + \frac{\partial G^{\mathrm{an},1}}{\partial \theta_1}\Big] \\
\pi^{\theta_2} &:= -\rho\frac{\partial G}{\partial \theta_2} = -\rho\xi(1-\alpha)\Big[-\frac{\mu_0 M^{\mathrm{sat}}}{\rho}\Big[\cos(\theta_2)H_x + \sin(\theta_2)H_y\Big] + \frac{\partial G^{\mathrm{an},2}}{\partial \theta_2}\Big] \\
\pi^{\theta_3} &:= -\rho\frac{\partial G}{\partial \theta_3} = -\rho(1-\xi)\alpha\Big[-\frac{\mu_0 M^{\mathrm{sat}}}{\rho}\Big[-\sin(\theta_3)H_x + \cos(\theta_3)H_y\Big] + \frac{\partial G^{\mathrm{an},3}}{\partial \theta_3}\Big] \\
\pi^{\theta_4} &:= -\rho\frac{\partial G}{\partial \theta_4} = -\rho\xi\alpha\Big[-\frac{\mu_0 M^{\mathrm{sat}}}{\rho}\Big[-\cos(\theta_4)H_x - \sin(\theta_4)H_y\Big] + \frac{\partial G^{\mathrm{an},4}}{\partial \theta_4}\Big]
\end{aligned}
\tag{16}
$$

The defined quantities $\tilde{\boldsymbol{\pi}}^{\mathrm{r}}$, $\tilde{\pi}^{\xi}$ and π^{α} can be interpreted as thermodynamic driving forces for the variant reorientation process and the magnetic domain wall motion, respectively. This fact will be discussed in more detail in the following subsection. The Clausius-Duhem inequality (7) can be reduced with the definition of the driving forces as follows

$$
\tilde{\boldsymbol{\pi}}^{\mathrm{r}}:\dot{\boldsymbol{\varepsilon}}^{\mathrm{r}} + \tilde{\pi}^{\xi}\dot{\xi} + \pi^{\alpha}\dot{\alpha} + \sum_{i=1}^{4}\pi^{\theta_i}\dot{\theta}_i \geq 0 \,, \tag{17}
$$

where temperature gradients have been considered negligible.

From physical observations it is reasonable to assume that the magnetization rotations are essentially thermodynamically reversible (Cullity, 1972; Kittel, 1949), and thus do not contribute to the entropy production. This is equivalent to stating that the driving forces for the respective magnetization rotations are identically zero, i. e.

$$
\pi^{\theta_i} := -\rho\frac{\partial G}{\partial \theta_i} = 0 \,. \tag{18}
$$

The entropy inequality (17) then reduces to

$$
\tilde{\boldsymbol{\pi}}^{\mathrm{r}}:\dot{\boldsymbol{\varepsilon}}^{\mathrm{r}} + \tilde{\pi}^{\xi}\dot{\xi} + \pi^{\alpha}\dot{\alpha} \geq 0 \,. \tag{19}
$$

Equations (18) represent a set of four relations to determine the four angles θ_i as functions of the independent state variables as well as the loading history.

3.2.3 Evolution of the reorientation strain and postulation of functions governing the activation of reorientation or domain wall motion processes

The remaining internal state variables $\boldsymbol{\varepsilon}^{\mathrm{r}}, \xi$ and α are, as evident from the local entropy production inequality (19), associated with energy dissipation. In this section evolution equations are derived for these internal

variables based on the principle of maximum dissipation for dissipative processes.

In modeling of conventional shape memory behavior the transformation strain is usually related to the martensitic volume fraction (Boyd and Lagoudas, 1996; Lagoudas et al., 1996; Bo and Lagoudas, 1999). Following this approach, the evolution of the reorientation strain associated with the magnetic shape memory effect is proposed to be proportional to the rate of change of the martensitic variant volume fraction

$$\dot{\boldsymbol{\varepsilon}}^{\mathrm{r}} = \boldsymbol{\Lambda}^{\mathrm{r}} \dot{\xi} \, . \tag{20}$$

The reorientation strain is therefore no longer an independent internal state variable. In the equation above $\boldsymbol{\Lambda}^{\mathrm{r}}$ is the reorientation strain tensor defining the direction in which the reorientation strain develops based on the direction of the applied magnetic field. It can in general be a function of the applied stress. An explicit form of the tensor will be given in Section 4.1 for a specific example. For the special case of constant $\boldsymbol{\Lambda}^{\mathrm{r}}$ expression (20) can be integrated to yield the reorientation strain, so that the total strain, according to (2) and (15b), is then given by

$$\boldsymbol{\varepsilon} = \mathcal{S}\boldsymbol{\sigma} + \boldsymbol{\Lambda}^{\mathrm{r}} \xi + \bar{\boldsymbol{\varepsilon}}^{\mathrm{tr}} \, . \tag{21}$$

If $\boldsymbol{\Lambda}^{\mathrm{r}}$ is not constant, i. e. if the applied stress is not constant, equation (20) has to be used incrementally (Qidwai and Lagoudas, 2000a).

If one further defines the total thermodynamic driving force for the twin boundary motion associated with the variant reorientation process as

$$\pi^{\xi} := \boldsymbol{\sigma}^{\mathrm{eff}} : \boldsymbol{\Lambda}^{\mathrm{r}} - \rho \frac{\partial G}{\partial \xi} = \tilde{\boldsymbol{\pi}}^{\mathrm{r}} : \boldsymbol{\Lambda}^{\mathrm{r}} + \tilde{\pi}^{\xi} \, , \tag{22}$$

the Clausius-Duhem inequality (19), by utilizing equations (16) and (20), can finally be written as

$$\pi^{\xi} \dot{\xi} + \pi^{\alpha} \dot{\alpha} \geq 0 \, . \tag{23}$$

From this form of the inequality it is evident that the driving forces π^{ξ} and π^{α} are thermodynamically conjugate to the internal state variables ξ and α, respectively. It is assumed that the dissipative processes associated with the motion of twin boundaries and the motion of magnetic domain walls are decoupled, so that both terms of the left hand side of (23) need to satisfy the inequality separately.

We can then proceed to define a *reorientation function* in terms of the thermodynamic driving force π^{ξ} as

$$\Phi^{\xi}(\boldsymbol{\sigma}, \mathbf{H}, \xi, \alpha) = \begin{cases} \pi^{\xi} - Y^{\xi} \, , & \dot{\xi} > 0 \\ -\pi^{\xi} - Y^{\xi} \, , & \dot{\xi} < 0 \end{cases} \, , \tag{24}$$

where the dependence on the rotation angles θ_j is assumed to have been eliminated by using the constraints (12). The proposed reorientation function is similar to transformation functions used in the modeling of rate independent phenomenological modeling of conventional shape memory behavior (Lagoudas et al., 1996; Qidwai and Lagoudas, 2000a). This function defines the extent of the elastic domain in the space of independent state variables, or conversely, critical values of the thermodynamic driving force for the start and finish of the reorientation process. The positive scalar quantity Y^{ξ} is physically related to internal dissipation associated with twin boundary motion. It is assumed that the reorientation process is subject to constraints derived from a principle of maximum reorientation dissipation, which can be expressed in terms of the Kuhn-Tucker or reorientation conditions

$$\begin{aligned} &\dot{\xi} \geq 0, \quad \Phi^{\xi}(\boldsymbol{\sigma}, \mathbf{H}, \xi, \alpha) \leq 0, \quad \Phi^{\xi} \dot{\xi} = 0 \, , \\ &\dot{\xi} \leq 0, \quad \Phi^{\xi}(\boldsymbol{\sigma}, \mathbf{H}, \xi, \alpha) \leq 0, \quad \Phi^{\xi} \dot{\xi} = 0 \, . \end{aligned} \tag{25}$$

Note that in the elastic regime where $\Phi^{\xi} < 0$ conditions (25) require $\dot{\xi} = 0$. The forward reorientation process is characterized by $\Phi^{\xi} = 0$ and $\dot{\xi} > 0$, whereas for the reverse process the conditions $\Phi^{\xi} = 0$ and $\dot{\xi} < 0$ hold. Since the thermodynamic driving force π^{ξ}, and therefore the reorientation function Φ^{ξ}, contain the hardening function f^{ξ}, the reorientation conditions (25) depend on the martensitic variant volume fraction and thereby on the loading history.

In an analogous manner one can postulate a function associated with the magnetic domain wall motion

$$\Phi^{\alpha}(\boldsymbol{\sigma}, \mathbf{H}, \xi, \alpha) = \begin{cases} \pi^{\alpha} - Y^{\alpha}, & \dot{\alpha} > 0 \\ -\pi^{\alpha} - Y^{\alpha}, & \dot{\alpha} < 0 \end{cases} . \tag{26}$$

The conditions governing the activation of the magnetic domain wall motion process are then given by

$$\begin{aligned} &\dot{\alpha} \geq 0, \quad \Phi^{\alpha}(\boldsymbol{\sigma}, \mathbf{H}, \xi, \alpha) \leq 0, \quad \Phi^{\alpha}\dot{\alpha} = 0 , \\ &\dot{\alpha} \leq 0, \quad \Phi^{\alpha}(\boldsymbol{\sigma}, \mathbf{H}, \xi, \alpha) \leq 0, \quad \Phi^{\alpha}\dot{\alpha} = 0 . \end{aligned} \tag{27}$$

4 Application of the MSMA Constitutive Model

4.1 Reduction of the model equations for a 2-D special case

In the derivation of the constitutive model for MSMA in Section 3.2 the incorporation of the magnetic domain wall motion and the magnetization rotation have been discussed in detail. For the sake of simplicity, two assumptions are made for the special numerical example to be considered here. First, this case is restricted to the modeling of the variant reorientation process with a fixed magnetic domain structure of $\alpha = 1$ (for $|\mathbf{H}| > 0$). Thus one magnetic domain is eliminated completely at the expense of the more favorably oriented domain, and magnetic domain walls are therefore not present.

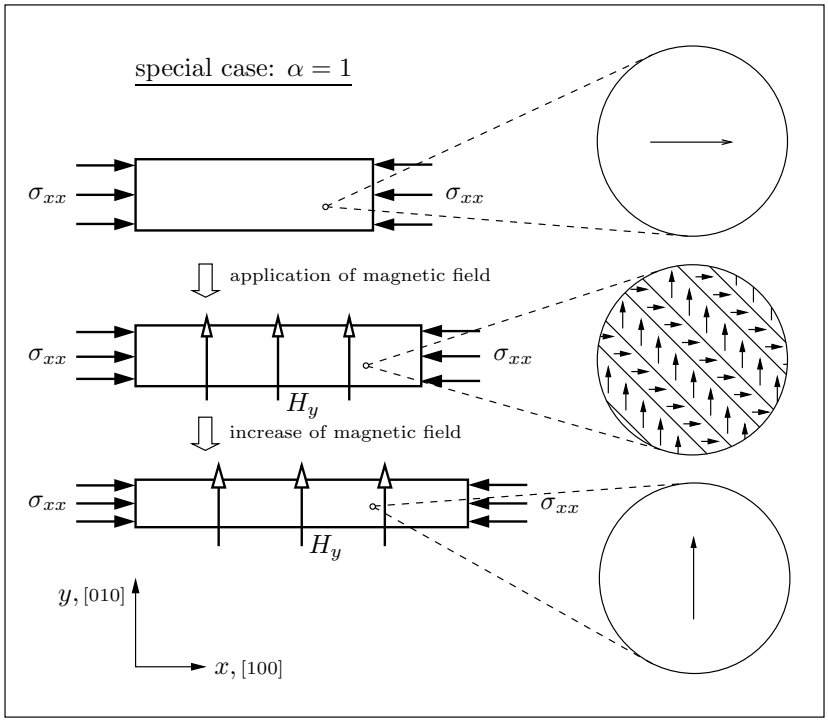

Figure 9: The variant reorientation process with fixed domain structure $\alpha = 1$.

The assumption of single domain configurations has often been made in the literature, and has in fact been supported by reported observations that after the application of relatively low magnetic fields ($H > 100\,\mathrm{Oe} = 7.9\,\mathrm{kAm}^{-1}$), 180°-domain walls are essentially eliminated (Tickle, 2000; O'Handley et al., 2003). The second assumption to restrict this numerical example is that of infinite magnetic anisotropy, which also has quite often been used in the literature. This inhibits the rotation of the magnetization vectors with respect to the magnetic easy axes. As will be evident from the numerical results, this assumption yields good predictions if one is only interested in the nonlinear strain response, not the prediction of magnetization curves. A more complex example, in which the rotation of magnetization is permitted, has

recently been studied in Kiefer and Lagoudas (2005), to which the reader is referred for more details on the implications of magnetization rotation, in particular on the predictability of the magnetization hysteresis curves.

The implication of the assumptions made for the special case of concern here is that changes of the magnetization are due only to the redistribution of martensitic variants. The assumed nature of the magnetic and crystallographic microstructure is schematically illustrated in Figure 9, which represents a modification of Figure 2 for the case of fixed magnetic microstructure. Recall that this 2-D set up, which illustrates the magnetic shape memory effect, has been discussed in Section 2.1.
In the case of $\alpha=1$ and $\theta_i=0$ the free energy expression (14) reduces to

$$G = -\frac{1}{2\rho}\,\boldsymbol{\sigma}:\mathcal{S}\boldsymbol{\sigma} - \frac{\mu_0}{\rho}M^{\mathrm{sat}}\Big[(1-\xi)\mathbf{e}_x + \xi\mathbf{e}_y\Big]\cdot\mathbf{H} + \frac{1}{\rho}\,f^{\xi}(\xi,\boldsymbol{\varepsilon}^{\mathrm{r}}) + G_0(T)\ . \tag{28}$$

The constitutive equations for the dependent state variables (15), and the thermodynamic driving force for twin boundary motion (22), using (16a,b), reduce to

$$\begin{aligned}
s &= -\frac{\partial G}{\partial T} = -\frac{\partial G_0}{\partial T} = \text{const}\ ,\\
\boldsymbol{\varepsilon}^{\mathrm{te}} &= -\rho\frac{\partial G}{\partial \boldsymbol{\sigma}} = \mathcal{S}\boldsymbol{\sigma}\ ,\\
\mathbf{M} &= -\frac{\rho}{\mu_0}\,\frac{\partial G}{\partial \mathbf{H}} = M^{\mathrm{sat}}\Big[(1-\xi)\mathbf{e}_x + \xi\mathbf{e}_y\Big]\ ,\\
\pi^{\xi} &= \boldsymbol{\sigma}^{\mathrm{eff}}:\boldsymbol{\Lambda}^{\mathrm{r}} - \rho\frac{\partial G}{\partial \xi} = \boldsymbol{\sigma}^{\mathrm{eff}}:\boldsymbol{\Lambda}^{\mathrm{r}} + \frac{1}{2}\,\boldsymbol{\sigma}:\Delta\mathcal{S}\boldsymbol{\sigma} - \mu_0 M^{\mathrm{sat}}[H_x - H_y] - \frac{\partial f^{\xi}}{\partial \xi}\ .
\end{aligned} \tag{29}$$

Expression (16c), the driving force associated with domain wall motion, has been omitted, since the magnetic microstructure can not evolve in the considered case. Since the local magnetization rotations are assumed to be inhibited, the dependence of the free energy on the rotation angles is eliminated and the associated driving forces (16d)-(16g) are equivalently equal to zero.

Recall that in the considered 2-D example the specimen is biased into a single variant 1 state by applying an axial stress, which is kept constant. An external, transverse magnetic field is used to favor martensitic 2, in which the magnetization is oriented along the transverse y-axis. The difference in crystallographic dimensions of the two variants results in the observed axial reorientation strain.

The material response is considered at a material point in a region of the specimen in which the measured fields are homogeneous. The stress state $\boldsymbol{\sigma}$ is then reasonably assumed to be uniaxial, i. e.

$$[\boldsymbol{\sigma}]_{ij} = \begin{bmatrix} \sigma & 0 & 0\\ 0 & 0 & 0\\ 0 & 0 & 0 \end{bmatrix}\ ,\ \text{with}\quad \sigma = \text{const} < 0 \quad\text{and}\quad \sigma^{\mathrm{sv}} < |\sigma| < \sigma^{\mathrm{b}}\ . \tag{30}$$

The magnetic field $\mathbf{H}$ has the components

$$[\mathbf{H}]_i = \begin{bmatrix} 0\\ H\\ 0 \end{bmatrix}, H \geq 0\ ; \quad \text{magnetic loading sequence: } H = \begin{cases} 0 \rightarrow H^{\max} & \text{(forward)}\\ H^{\max} \rightarrow 0 & \text{(reverse)}\ . \end{cases} \tag{31}$$

Recall that $\mathbf{H}$ is the magnetic field considered at the material point, which is reduced in magnitude compared to the externally applied field by the magnitude of the demagnetization field.

The reorientation strain is observed to develop in the axial direction, and is in the considered case of the explicit form

$$[\boldsymbol{\Lambda}^{\mathrm{r}}]_{ij} = \varepsilon^{\mathrm{r,max}}(\sigma)\begin{bmatrix} 1 & 0 & 0\\ 0 & -1 & 0\\ 0 & 0 & 0 \end{bmatrix}\ . \tag{32}$$

The reorientation strain does work against the biasing stress, which influences the stored energy in the system. This is reflected in the first term of the driving force for twin boundary motion, equation (22), which in the simplified case reduces to

$$\boldsymbol{\sigma}^{\mathrm{eff}} : \boldsymbol{\Lambda}^{\mathrm{r}} = \sigma \varepsilon^{\mathrm{r,max}} \,, \tag{33}$$

where it has been assumed that the hardening function (13), which is associated with the twin boundary motion in the variant reorientation process and therefore the Gibbs free energy, does not explicitly depend on the reorientation strain, so that in this case $\boldsymbol{\sigma}^{\mathrm{eff}} = \boldsymbol{\sigma}$.

With the simplifications (30), (31) and (33) the Gibbs free energy expression (28) and the driving force for variant reorientation (29d) reduce to the following expressions

$$\begin{aligned} G &= -\frac{1}{2\rho} S \sigma^2 - \frac{\mu_0}{\rho} M^{\mathrm{sat}} \xi H + \frac{1}{\rho} f^{\xi}(\xi, \boldsymbol{\varepsilon}^{\mathrm{r}}) + G_0(T) \,, \\ \pi^{\xi} &= \sigma \varepsilon^{\mathrm{r,max}} + \frac{1}{2} \Delta S \sigma^2 + \mu_0 M^{\mathrm{sat}} H - \frac{\partial f^{\xi}}{\partial \xi} \,, \end{aligned} \tag{34}$$

for this special case, where S is the simplified notation for the component $[\mathcal{S}]_{xxxx}$.

To complete the formulation of the constitutive model, the generically introduced hardening function (13) needs to be specified. Several types of hardening functions have been presented in the literature in the context of martensitic phase transformation of conventional shape memory alloys, such as the exponential hardening model (Tanaka, 1986; Sato and Tanaka, 1988), the polynomial hardening model (Lagoudas et al., 1996; Boyd and Lagoudas, 1996), and the trigonometric hardening model (Liang and Rogers, 1990; Lagoudas et al., 1996). The exponential hardening function is related to the nucleation process of martensite and was actually the first model introduced in the literature. The polynomial function is motivated by a series expansion of the free energy. The trigonometric hardening model has been introduced to better match results with experimental observations, which has been shown to yield good agreement between experimental results and model predictions in conventional SMAs.

The polynomial and the trigonometric hardening functions are adapted here in the context of the variant reorientation process. The reduced constitutive equations are utilized in the derivation of explicit evolution equations for the martensitic variant volume fraction, for two specific forms of the hardening function (13).

4.1.1 Evolution of the martensitic variant volume fraction: Quadratic polynomial hardening model

The quadratic polynomial hardening function associated with the variant reorientation process is given by

$$f^{\xi,\mathrm{p}}(\xi) = \begin{cases} \frac{1}{2} A^{\mathrm{p}} \xi^2 + (B_1^{\mathrm{p}} + B_2^{\mathrm{p}}) \xi \,, & \dot{\xi} > 0 \\ \frac{1}{2} C^{\mathrm{p}} \xi^2 + (B_1^{\mathrm{p}} - B_2^{\mathrm{p}}) \xi \,, & \dot{\xi} < 0 \end{cases} \,, \tag{35}$$

which yields

$$\frac{\partial f^{\xi,\mathrm{p}}}{\partial \xi} = \begin{cases} A^{\mathrm{p}} \xi + B_1^{\mathrm{p}} + B_2^{\mathrm{p}} \,, & \dot{\xi} > 0 \\ C^{\mathrm{p}} \xi + B_1^{\mathrm{p}} - B_2^{\mathrm{p}} \,, & \dot{\xi} < 0 \end{cases} \,, \tag{36}$$

where $A^{\mathrm{p}}, B_1^{\mathrm{p}}, B_2^{\mathrm{p}}$ and C^{p} are adjustable parameters of the quadratic polynomial hardening function. It will be shown in Section 4.2, how they can be connected to physically more meaningful and measurable quantities.

With the expression for the driving force given by (34b) and the derivative of the quadratic polynomial hardening function given by (36), it follows for the forward reorientation process, which is subject to the reorientation function (24) and the reorientation conditions (25):

reorientation $1 \rightarrow 2$ ($\dot{\xi} > 0$):

$$\pi^{\xi} = \sigma\varepsilon^{\mathrm{r,max}} + \frac{1}{2}\Delta S\sigma^2 + \mu_0 M^{\mathrm{sat}} H - A^{\mathrm{p}}\xi - B_1^{\mathrm{p}} - B_2^{\mathrm{p}} = Y^{\xi,\mathrm{p}} \,. \tag{37}$$

Because of the scalar nature of the internal variable ξ equation (37) can be solved directly to give the closed-form solution for the evolution of the variant 2 volume fraction

$$\xi^{(1,2)} = \frac{1}{A^{\mathrm{p}}}\left[\sigma\varepsilon^{\mathrm{r,max}} + \frac{1}{2}\Delta S\sigma^2 + \mu_0 M^{\mathrm{sat}} H - B_1^{\mathrm{p}} - B_2^{\mathrm{p}} - Y^{\xi,\mathrm{p}}\right] \,. \tag{38}$$

Similarly, for the reverse reorientation process one finds:

reorientation $2 \rightarrow 1$ ($\dot{\xi} < 0$):

$$\pi^{\xi} = \sigma\varepsilon^{\mathrm{r,max}} + \frac{1}{2}\Delta S\sigma^2 + \mu_0 M^{\mathrm{sat}} H - C\xi - B_1^{\mathrm{p}} + B_2^{\mathrm{p}} = -Y^{\xi,\mathrm{p}} \,, \tag{39}$$

and the evolution of the volume fraction is thus given by

$$\xi^{(2,1)} = \frac{1}{C^{\mathrm{p}}}\left[\sigma\varepsilon^{\mathrm{r,max}} + \frac{1}{2}\Delta S\sigma^2 + \mu_0 M^{\mathrm{sat}} H - B_1^{\mathrm{p}} + B_2^{\mathrm{p}} + Y^{\xi,\mathrm{p}}\right] \,. \tag{40}$$

4.1.2 Evolution of the martensitic variant volume fraction: Trigonometric hardening model

The trigonometric hardening function is of the form

$$f^{\xi,\mathrm{c}}(\xi) = \begin{cases} \displaystyle\int_0^{\xi} -A^{\mathrm{c}}\left[\pi - \cos^{-1}(2\tilde{\xi} - 1)\right] \mathrm{d}\tilde{\xi} + (B_1^{\mathrm{c}} + B_2^{\mathrm{c}})\xi \,, & \dot{\xi} > 0 \\ \displaystyle\int_0^{\xi} -C^{\mathrm{c}}\left[\pi - \cos^{-1}(2\tilde{\xi} - 1)\right] \mathrm{d}\tilde{\xi} + (B_1^{\mathrm{c}} - B_2^{\mathrm{c}})\xi \,, & \dot{\xi} < 0 \end{cases} \,, \tag{41}$$

and thus

$$\frac{\partial f^{\xi,\mathrm{c}}}{\partial \xi} = \begin{cases} -A^{\mathrm{c}}\left[\pi - \cos^{-1}(2\xi - 1)\right] + (B_1^{\mathrm{c}} + B_2^{\mathrm{c}}) \,, & \dot{\xi} > 0 \\ -C^{\mathrm{c}}\left[\pi - \cos^{-1}(2\xi - 1)\right] + (B_1^{\mathrm{c}} - B_2^{\mathrm{c}}) \,, & \dot{\xi} < 0 \end{cases} \,, \tag{42}$$

Using (34b) in combination with the derivative of the trigonometric hardening function (42) and the reorientation function (24) and reorientation conditions (25), one finds for the forward reorientation process:

reorientation $1 \rightarrow 2$ ($\dot{\xi} > 0$):

$$\pi^{\xi} = \sigma\varepsilon^{\mathrm{r,max}} + \frac{1}{2}\Delta S\sigma^2 + \mu_0 M^{\mathrm{sat}} H + A^{\mathrm{c}}\left[\pi - \cos^{-1}(2\xi - 1)\right] - B_1^{\mathrm{c}} - B_2^{\mathrm{c}} = Y^{\xi,\mathrm{c}} \,. \tag{43}$$

The closed-form solution for the evolution of the variant volume fraction for the trigonometric hardening model is derived to be

$$\xi^{(1,2)} = \frac{1}{2}\cos\left(-\frac{1}{A^{\mathrm{c}}}\left[-\sigma\varepsilon^{\mathrm{r,max}} - \frac{1}{2}\Delta S\sigma^2 - \mu_0 M^{\mathrm{sat}} H + B_1^{\mathrm{c}} + B_2^{\mathrm{c}} + Y^{\xi,\mathrm{c}}\right] + \pi\right) + \frac{1}{2} \,. \tag{44}$$

For the reverse reorientation process it follows:

reorientation $2 \rightarrow 1$ ($\dot{\xi} < 0$):

$$\pi^{\xi} = \sigma\varepsilon^{\mathrm{r,max}} + \frac{1}{2}\Delta S\sigma^2 + \mu_0 M^{\mathrm{sat}} H + C^{\mathrm{c}}\left[\pi - \cos^{-1}(2\xi - 1)\right] - B_1^{\mathrm{c}} + B_2^{\mathrm{c}} = -Y^{\xi,\mathrm{c}} \,. \tag{45}$$

and thus

$$\xi^{(2,1)} = \frac{1}{2}\cos\left(-\frac{1}{C^{\mathrm{c}}}\left[-\sigma\varepsilon^{\mathrm{r,max}} - \frac{1}{2}\Delta S\sigma^2 - \mu_0 M^{\mathrm{sat}} H + B_1^{\mathrm{c}} - B_2^{\mathrm{c}} - Y^{\xi,\mathrm{c}}\right] + \pi\right) + \frac{1}{2} \,. \tag{46}$$

4.2 Determination of model parameters

Four hardening parameters A, C, B_1 and B_2 as well as the critical value for the driving force Y^{ξ} have been introduced for each of the two hardening models. These model parameters can more conveniently be expressed in terms of the measurable magnetic field values $H^{\mathrm{s}(1,2)}(\sigma^*)$, $H^{\mathrm{f}(1,2)}(\sigma^*)$, $H^{\mathrm{s}(2,1)}(\sigma^*)$ and $H^{\mathrm{f}(2,1)}(\sigma^*)$, which correspond to the onset and termination of the forward and reverse reorientation process (cf. Figure 3), and are considered material constants. These five parameters are directly obtained by the acquisition of data from a **single** constant-stress hysteresis loop at the arbitrary stress level σ^* , where $\sigma^{\mathrm{sv}} < \sigma^* < \sigma^{\mathrm{b}}$. To be more specific, in order to determine the necessary model parameters, an experimentally measured strain vs. magnetic field hysteresis loop, such as the ones qualitatively shown in Figure 3, is needed. Data corresponding to reorientation experiments of this type have been published in the literature (Tickle et al., 1999; Tickle, 2000). The procedure is to choose one particular curve from which the parameters are to be determined. Then, the respective magnetic field values for the activation of the reorientation process need to be estimated from this curve. Tangent lines to different points of the hysteresis loop can be used for a methodical procedure of finding these magnetic field strength values. The remaining input is the value of the blocking stress and the dependence of the maximum reorientation strain $\varepsilon^{\mathrm{r,max}}$ on the applied bias stress, for the tested MSMA material.

Polynomial Hardening Model	Trigonometric (Cosine) Hardening Model
$A^{\mathrm{p}} = \mu_0 M^{\mathrm{sat}} \big(H^{\mathrm{f}(1,2)}(\sigma^*) - H^{\mathrm{s}(1,2)}(\sigma^*) \big)$	$A^{\mathrm{c}} = \frac{\mu_0 M^{\mathrm{sat}}}{\pi} \big(H^{\mathrm{s}(1,2)}(\sigma^*) - H^{\mathrm{f}(1,2)}(\sigma^*) \big)$
$B_1^{\mathrm{p}} = \frac{1}{2}\mu_0 M^{\mathrm{sat}} \big(H^{\mathrm{s}(1,2)}(\sigma^*) + H^{\mathrm{f}(2,1)}(\sigma^*) \big)$ $+\sigma^* \, \varepsilon^{\mathrm{r,max}}(\sigma^*)$	$B_1^{\mathrm{c}} = \frac{1}{2}\mu_0 M^{\mathrm{sat}} \big(H^{\mathrm{s}(1,2)}(\sigma^*) + H^{\mathrm{f}(2,1)}(\sigma^*) \big)$ $+\sigma^* \, \varepsilon^{\mathrm{r,max}}(\sigma^*)$
$B_2^{\mathrm{p}} = \frac{1}{4} \big(C^{\mathrm{p}} - A^{\mathrm{p}} \big)$	$B_2^{\mathrm{c}} = \frac{\pi}{4} \big(A^{\mathrm{c}} - C^{\mathrm{c}} \big)$
$C^{\mathrm{p}} = \mu_0 M^{\mathrm{sat}} \big(H^{\mathrm{s}(2,1)}(\sigma^*) - H^{\mathrm{f}(2,1)}(\sigma^*) \big)$	$C^{\mathrm{c}} = \frac{\mu_0 M^{\mathrm{sat}}}{\pi} \big(H^{\mathrm{f}(2,1)}(\sigma^*) - H^{\mathrm{s}(2,1)}(\sigma^*) \big)$
$Y^{\xi,\mathrm{p}} = \frac{1}{2}\mu_0 M^{\mathrm{sat}} \big(H^{\mathrm{s}(1,2)}(\sigma^*) - H^{\mathrm{f}(2,1)}(\sigma^*) \big) - B_2^{\mathrm{p}}$	$Y^{\xi,\mathrm{c}} = \frac{1}{2}\mu_0 M^{\mathrm{sat}} \big(H^{\mathrm{s}(1,2)}(\sigma^*) - H^{\mathrm{f}(2,1)}(\sigma^*) \big) - B_2^{\mathrm{c}}$

Table 1: Relation between material constants and model parameters in the cases of polynomial and trigonometric hardening.

The model parameters are then obtained by using the specific relations to the measured quantities listed in Table 1. These relations have been derived by using the reduced expressions for the driving force during reorientation (37) and (39), for the quadratic polynomial hardening model, as well as (43) and (45), for the trigonometric hardening case. For example, the activation of the forward reorientation process with polynomial hardening is described by equation (37) when substituting $\xi = 0$. The resulting expression can be solved for a relation of type $H(\sigma)$. For the specific stress level σ^*, corresponding to the curve by which the parameters are adjusted, the equation $H(\sigma^*, \xi = 0) = H^{\mathrm{s}(1,2)}(\sigma^*)$ must hold. This results in the first relation between the hardening parameters and the measured quantities. Three more conditions of this kind follow from the driving force expressions by substituting the values of $\xi = 0$ and $\xi = 1$, respectively. The final relation needed to determine the five independent model parameters stems from the condition of continuity of the hardening functions (35) and (41) at $\xi = 1$, at which the sign of the evolution rate $\dot{\xi}$ changes for the forward and reverse reorientation process.

4.3 Numerical results

A numerical example is now presented for the considered special case in which the magnetic shape memory effect is induced in a stress biased NiMnGa single crystal specimen under the application of an external magnetic field. The reduced equations for the MSMA constitutive model have been presented in Section 4.1. The model parameters have been determined by utilizing the procedure outlined in the previous subsection 4.2, based on experimental data published by Tickle (2000) for the considered Ni_2MnGa magnetic shape

memory alloy single crystals.[3] They are listed in Table 2, for both hardening functions. The magnetic field threshold values for the reorientation process have been obtained from data corresponding to a strain-magnetic field hysteresis loop under a biasing stress of $-1.0\,\mathrm{MPa}$.[4] The model parameters for the polynomial and the trigonometric hardening functions have been determined using the relations introduced in Table 1.

Quantitiy	Value (unit)
ρ	$8300.0\,\mathrm{kg\,m^{-3}}$
α	1.0/0.0
ΔS	$0.0\,\mathrm{Pa^{-1}}$
μ_0	$1.256\,\mu\mathrm{NA^{-2}}$
M^{sat}	$622.0\,\mathrm{kAm^{-1}}$
σ^*	$-1.0\,\mathrm{MPa}$
$H^{\mathrm{s}(1,2)}(\sigma^*)$	$238.8\,\mathrm{kAm^{-1}}$
$H^{\mathrm{f}(1,2)}(\sigma^*)$	$1250.0\,\mathrm{kAm^{-1}}$
$H^{\mathrm{s}(2,1)}(\sigma^*)$	$398.0\,\mathrm{kAm^{-1}}$
$H^{\mathrm{f}(2,1)}(\sigma^*)$	$15.9\,\mathrm{kAm^{-1}}$
$\varepsilon^{\mathrm{r,max}}(-1\,\mathrm{MPa})$	0.02148
$\varepsilon^{\mathrm{r,max}}(-3\,\mathrm{MPa})$	0.0133
$\varepsilon^{\mathrm{r,max}}(-5\,\mathrm{MPa})$	0.0034
$\varepsilon^{\mathrm{r,max}}(-7\,\mathrm{MPa})$	0.00035
σ^{b}	$-8\,\mathrm{MPa}$

Parameter	Value (unit)
Polynomial Hardening Model	
A^{p}	$0.789982\,\mathrm{MPa}$
B_1^{p}	$0.078018\,\mathrm{MPa}$
B_2^{p}	$-0.122872\,\mathrm{MPa}$
C^{p}	$0.298493\,\mathrm{MPa}$
$Y^{\xi,\mathrm{p}}$	$0.209933\,\mathrm{MPa}$
Trigonometric Hardening Model	
A^{c}	$-0.251459\,\mathrm{MPa}$
B_1^{c}	$0.078018\,\mathrm{MPa}$
B_2^{c}	$-0.122872\,\mathrm{MPa}$
C^{c}	$-0.095013\,\mathrm{MPa}$
$Y^{\xi,\mathrm{c}}$	$0.209933\,\mathrm{MPa}$

Table 2: Material constants for a Ni_2MnGa specimen and the resulting model parameters for both hardening functions.

The remaining input to the model is the stress dependence of the maximum reorientation strain. Recall that the maximum reorientation strain values for different bias stress levels are reflected in the variation of hysteresis loop sizes, as qualitatively illustrated by Figure 3. Figure 10 shows experimental $\varepsilon^{\mathrm{r,max}}(\sigma)$-data (diamonds) as published in Tickle (2000) for certain stress levels, whose numerical values have also been listed in Table 2. Based on these data points a polynomial curve-fit has been calculated, represented by the solid line in Figure 10, whose explicit functional form is given by

$$\varepsilon^{\mathrm{r,max}}(\sigma) = \begin{cases} -(0.387798\cdot 10^{-28})\sigma^4 - (0.799018\cdot 10^{-21})\sigma^3 - (0.515693\cdot 10^{-14})\sigma^2 \\ -(0.770170\cdot 10^{-8})\sigma + 0.018175 & , \sigma^{\mathrm{b}} \le \sigma \le 0 \\ 0 & , \sigma < \sigma^{\mathrm{b}} \end{cases} . \quad (47)$$

[3]Recall that the experimentally measured strain vs. applied magnetic field curves can not be interpreted as the constitutive response of the MSMA material, since the applied magnetic field depends on the specimen geometry through the demagnetization factor. In order to extract the constitutive response from experimental data, one has to compute the corresponding strain vs. internal magnetic field curves by subtracting demagnetization field from the applied field. However, since the demagnetizing field depends on the magnetization, the corresponding magnetization curves need to be considered simultaneously. The matter is complicated by the fact that the measured magnetization curves are themselves given in terms of the applied magnetic field, not the internal magnetic at a specific material point. Since not all of the necessary data needed to extract these curves is provided in Tickle (2000), the parameters for this numerical application example are determined based on the measured strain vs. applied magnetic field curves, which in this case are just interpreted as the constitutive response. This assumption only limits the predictability of quantitative data for this specific experiment, the procedure is, however, sufficient to illustrate the applicability and validity of the proposed constitutive model as well as the presented method of determining model parameters.

[4]Throughout this paper SI-units are used. However, the CGS-unit system is more commonly used in the literature on magnetic materials. For the magnetic field strength the conversion factor $1\,\mathrm{Oe} \mathrel{\hat{=}} 79.6\,\mathrm{Am^{-1}}$ applies (Cullity, 1972). Despite being of same unit as the magnetic field strength in the SI-unit system, $\mathrm{emu\,cm^{-3}}$ is the commonly used unit for the magnetization in the CGS-system. The corresponding conversion factors are given by: $1\,\mathrm{emu\,cm^{-3}} \mathrel{\hat{=}} 12.57\cdot 10^{-4}\,\mathrm{T}$ and $1\,\mathrm{T} \mathrel{\hat{=}} \mu_0^{-1}\,\mathrm{Am^{-1}}$. For example, the following material constants, as specified in Table 2, are converted to CGS-units as: $H^{\mathrm{s}(1,2)} = 3460\,\mathrm{Oe}$ and $M^{\mathrm{sat}} = 75\,\mathrm{emu\,g^{-1}}$.

The decline of the maximum reorientation strain exhibited by this particular polynomial fit at applied stress levels in the range of $\sigma^* \leq \sigma \leq 0$, for which no data points are available in (Tickle, 2000), is considered physically reasonable as it is observed in similar experiments (Karaman, 2004).

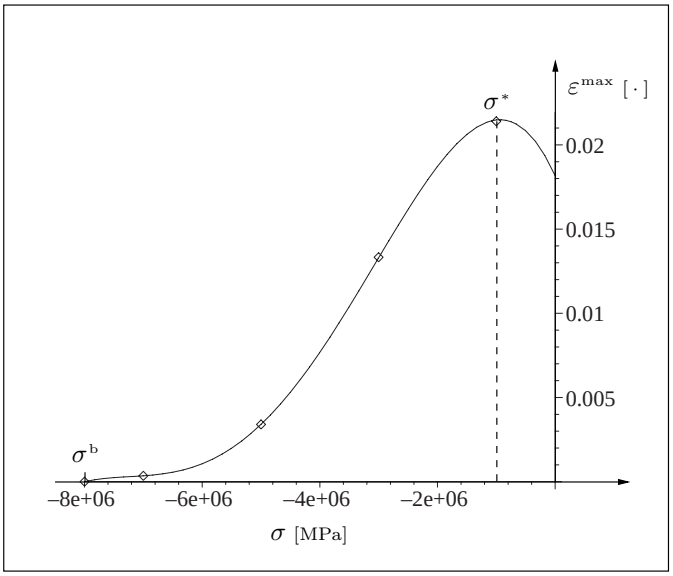

Figure 10: Stress dependence of the maximum magnetically induced reorientation strain. Shown are experimental data (Tickle, 2000) corresponding to different bias stress values (diamonds), and the approximated functional dependence used in the numerical example (solid line).

Note that this is the only instance in the procedure of applying the model to this specific example in which actual curve-fitting is utilized. This is done to accurately introduce the maximum reorientation strain as **input** to the model. With the phenomenological approach taken in this paper, the maximum transformation strain can not be predicted. A model intended to make such predictions has to include the analysis of the reorientation process at smaller length scales and account for the martensitic microstructure, for example, by considering the kinematics of twinning and detwinning in MSMA martensite.

With the set of model parameters specified, the stress dependent reorientation conditions can be graphically interpreted in terms of a phase diagram in axial stress-transverse magnetic field-space as seen in Figure 11. The depicted curves indicate the onset and termination of the forward, $H^{\mathrm{s}(1,2)}(\sigma_{xx})$ and $H^{\mathrm{f}(1,2)}(\sigma_{xx})$, as well as the reverse, $H^{\mathrm{s}(2,1)}(\sigma_{xx})$ and $H^{\mathrm{f}(2,1)}(\sigma_{xx})$, reorientation process, respectively.

Recall that, as explained in Section 4.2 in the context of determining model parameters, the explicit expressions of type $H_y(\sigma_{xx})$, by which the phase diagram is constructed, can be derived from the reduced reorientation conditions (37) and (39), for polynomial hardening, or (43) and (45), for the trigonometric hardening model by substituting the volume fractions of $\xi = 0$ and $\xi = 1$, respectively. In a full magnetic field cycle at a constant biasing stress of σ^*, the reorientation start and finish lines are crossed at the characteristic values $H^{\mathrm{s}(1,2)}(\sigma^*)$, $H^{\mathrm{f}(1,2)}(\sigma^*)$, $H^{\mathrm{s}(2,1)}(\sigma^*)$ and $H^{\mathrm{f}(2,1)}(\sigma^*)$, indicated by $(\times)$-symbols in Figure 11, which represent the data used in determining the model parameters (cf. Table 1 and Table 2). The shape and spacing of the reorientation start and finish surfaces is directly related to the parameters introduced with the hardening function (35), in the case of polynomial hardening, and (41), for the trigonometric hardening function, and is influenced by the stress dependence of the maximum reorientation strain (47). Corresponding phase diagrams in stress-temperature space have traditionally been utilized in the modeling of conventional shape memory alloys (Lagoudas et al., 1996; Qidwai and Lagoudas, 2000a). Phase diagrams similar to the one presented in Figure 11 have been constructed in the literature (Tickle et al., 1999). Phase diagrams have also been utilized in the discussion of the influence of magnetic fields on the martensitic phase transformation in magnetic shape memory alloys (Liang et al., 2002).

The slopes of the reorientation activation lines in the phase diagram can be expressed in the form of a

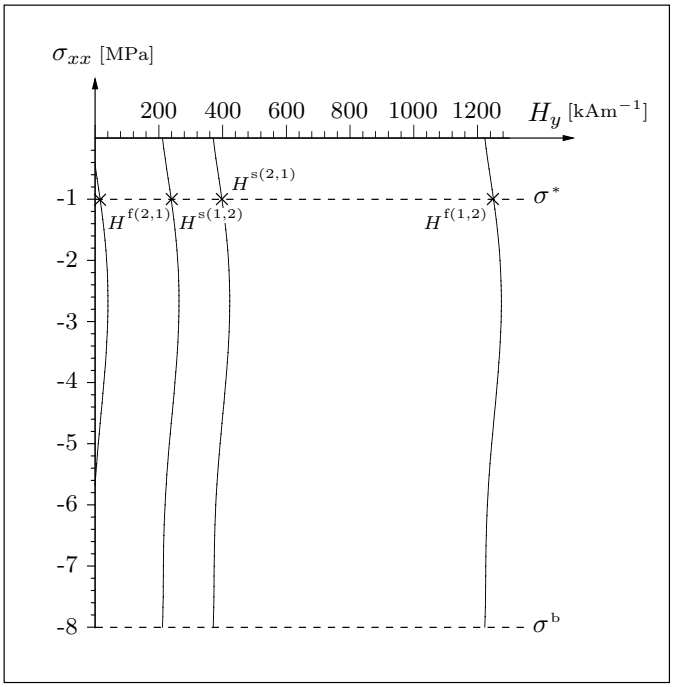

Figure 11: Numerical phase diagram for the variant reorientation process in the Ni_2MnGa alloy specified in Table 2. Displayed are the reorientation start and finish surfaces for the forward and reverse direction, respectively.

Clausius-Clapeyron type relation, which is deduced from equation (34b), as

$$\frac{\mathrm{d}\sigma}{\mathrm{d}H} = -\frac{\mu_0 M^{\mathrm{sat}}}{\varepsilon^{\mathrm{r,max}} + \sigma \frac{\mathrm{d}\varepsilon^{\mathrm{r,max}}}{\mathrm{d}\sigma}} \,. \tag{48}$$

Note that the model predicts a coupling between the stress dependence of the maximum reorientation strain and the slopes of the reorientation start and finish lines in the phase diagram. This is evident in the vertical slopes exhibited by the reorientation lines corresponding to stress levels at which the denominator of equation (48) vanishes. This occurs when i) both terms in the denominator balance each other or ii) both terms are zero. The latter case coincides with the blocking stress if the slope of $\varepsilon^{\mathrm{r,max}}(\sigma)$ also vanishes there. Initially, at low applied stress levels, the activation lines follow the straight lines predicted by Tickle et al. (1999), whose expression for the slope, translated into the notation used in this paper, is given by

$$\frac{\mathrm{d}\sigma}{\mathrm{d}H} = -\frac{\mu_0 M^{\mathrm{sat}}}{\varepsilon^{\mathrm{r,max}}} \,. \tag{49}$$

However, on account of the considered stress dependence of the maximum reorientation strain, reflected in the term $\sigma \frac{\mathrm{d}\varepsilon^{\mathrm{r,max}}}{\mathrm{d}\sigma}$ of the slope expression (48), a deviation from the straight lines is predicted by the presented model. It is actually observed in the considered experimental data (Tickle, 2000) that the magnetic field threshold values for the reorientation process do not vary linearly with the applied stress. The experimental activation curves are much better reflected by the predicted phase diagram of Figure 11.

Figure 12 shows a plot of the numerical strain vs. magnetic field response curves, such as the ones qualitatively introduced in Figure 3, based on the proposed MSMA constitutive model for both hardening laws. Dashed curves represent numerical results with quadratic polynomial hardening, while solid curves correspond to trigonometric hardening. Note that the vertical axis displays the reorientation strain, not the total strain, so that the depicted curves begin at a strain value of zero. Three exemplary curves for varying bias stress levels have been computed based on the model parameters specified in Table 2. The ε-H-hysteresis loop for the $-1.0\,\mathrm{MPa}$ compressive axial stress represents the simulation of the curve on the basis of which the model parameters were obtained. The remaining two loops are predictions of the constitutive response by the model. The reduced model equations describing the evolution of the martensitic volume fraction have

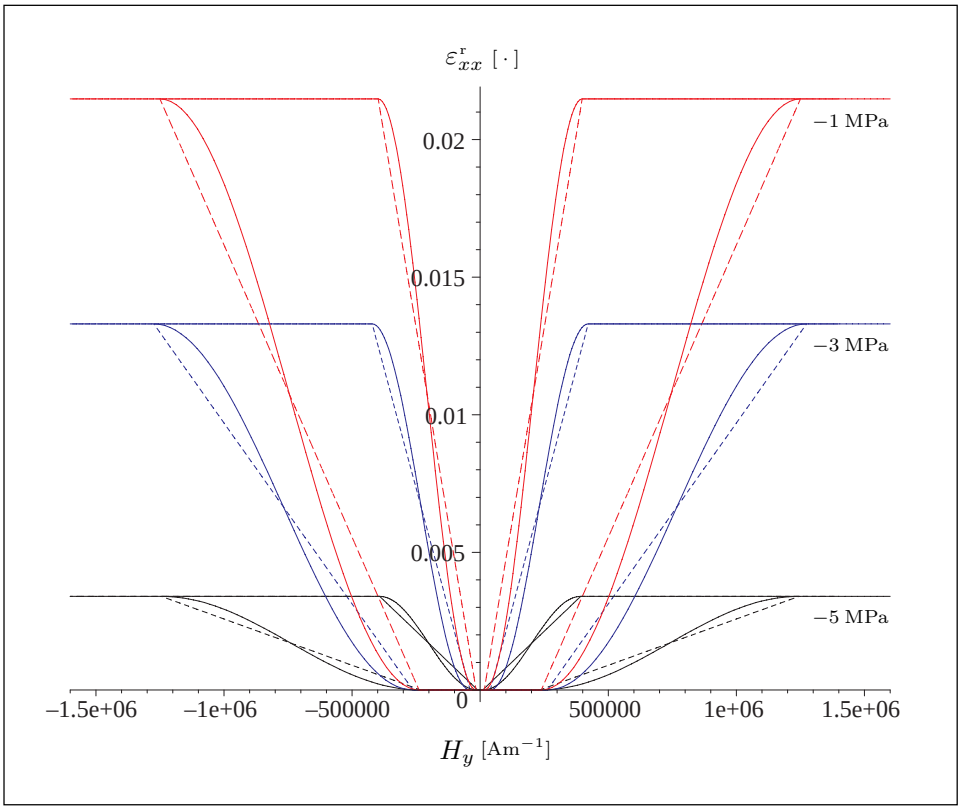

Figure 12: Axial reorientation strain vs. transverse magnetic field for different bias stress levels. Compared are the polynomial (dashed lines) and trigonometric (solid lines) hardening model predictions.

been presented in (38) and (40), for polynomial hardening, and in (44) and (46), for the trigonometric hardening model. Recall that the activation of the variant reorientation process is governed by the reorientation function (24), and is subject to the reorientation conditions (25). The evolution of the martensitic volume fraction is connected to the reorientation strain through the relation obtained by integrating equation (20). The hysteresis loops for negative magnetic fields ($-H^{\max} \leq H \leq 0$) have been computed based on a set of reduced equations for the assumption of $\alpha = 0$. These were derived in a procedure analogous to that presented in Section 4.1 for the assumption $\alpha = 1$. Physically this assumption means that with the application of an external magnetic field in the opposite direction, the magnetization direction of the specimen is instantaneously switched (i. e. $M_x = M^{\mathrm{sat}} \rightarrow -M^{\mathrm{sat}}$, $M_y = 0$, at $-H^{\max} \ll H < 0$) by magnetic domain wall motion.

In order to gauge the accuracy of the model predictions, Figure 13 compares the curves of the trigonometric hardening model (solid lines) to the experimental data (dashed lines) published by Tickle (2000) on which the model parameters for this example are based. It is evident that the numerical predictions capture the characteristic features of the macroscopic strain response related to the magnetic shape memory effect reasonably well, even with the assumption of fixed magnetic domain volume fractions and fixed magnetization directions made in this numerical example. Note in particular the predicted nonlinearity of the constitutive response and the predicted stress dependence of the size and shape of the hysteresis loops. The latter are closely connected to the computed reorientation activation surfaces depicted in the phase diagram (Figure 11), which in turn are influenced by the stress dependence of the maximum reorientation strain.

Some comments ought to be made regarding the exhibited discrepancies between the model prediction and the experimental data. First of all, it is observed that, as expected, the trigonometric hardening function captures the nonlinear evolution of the reorientation strain exhibited by the experimental data quite accurately, whereas the quadratic polynomial hardening model predicts a linear response in the reorientation regions. One possibility to further improve the accuracy of the predictions is to choose higher order polynomials or even different types of hardening functions. Due to the sparseness of experimental data the authors

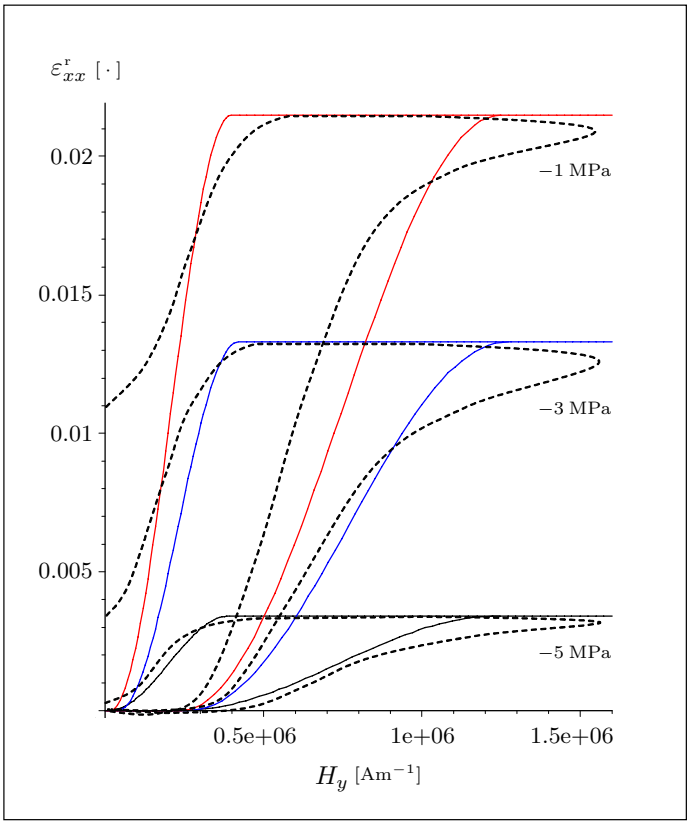

Figure 13: Comparison of the trigonometric hardening model curves (solid lines) and the experimental data (dashed lines) reported by Tickle (2000).

decided against increasing the level of complexity of the hardening functions at this point, since other effects may need to be incorporated first by alleviating some of the restricting assumptions made in this example.

Furthermore, it would be desirable to compare model predictions to experimental curves corresponding to a cycle in which the maximum reorientation strain has stabilized. Recall that it is usually observed in these experiments that the maximum reorientation strain changes in the first cycle, but in the second and subsequent cycles the value saturates (Karaman, 2004). It can be concluded that the considered experimental data does in fact not correspond to a stable cycle because the hysteresis curves intercept the strain axis at positive values, indicating that the reorientation strain is not fully recovered upon removal of the magnetic field. The model is not designed to capture this effect, but data for a stable cycle was not available at this point.

5 Discussion

In this paper the magnetic shape memory effect, as caused by the martensitic variant reorientation under externally applied magnetic fields, has been investigated. The associated macroscopic straining and magnetization response of the MSMA material has been discussed in detail. It has been demonstrated that the assumptions made with respect to the identification of the underlying microstructural and micromagnetic mechanisms causing the macroscopic material behavior, have led to a formulation which produces reasonable predictions of the strain response associated with the magnetic shape memory effect. An extended thermodynamic framework for phenomenological constitutive modeling has been presented. A specific free energy function has been proposed with a dependence on microstructurally motivated internal state variables, namely the martensitic variant and magnetic domain volume fractions, which account for dissipative effects and loading history dependence in the model. The rotation angles between magnetic easy axes and

the local magnetization directions have been introduced as additional internal state variables. Due to the reversible nature of the local magnetization rotation, is has been assumed that this process does not contribute to the entropy production, which leads to the implication that the thermodynamic driving forces associated with these internal state variables must vanish. From the free energy expression constitutive equations have been deduced by using appropriate thermodynamic relations. Equations governing the evolution of the martensitic variant volume fraction have been derived on the basis of a reorientation function and associated reorientation conditions, which determine the activation of the reorientation process. The correlated nonlinear evolution of the reorientation strain has been connected to the evolution of the variant volume fraction, where its direction is prescribed by the introduced reorientation strain tensor. Two types of hardening functions have been utilized.

For a special case of fixed magnetic domain structure and inhibited magnetization rotation, the established model has successfully been applied to predicting the magnetic shape memory effect. In a numerical example, based on data taken from the literature, strain-magnetic field response curves have been predicted, which exhibit all of the important features of the MSMA constitutive behavior connected to the variant reorientation process under applied magnetic and mechanical loading. In particular, the model captures the nonlinear and hysteretic nature of the reorientation strain response, as well as the stress dependence of the shape and size of the hysteresis. A detailed procedure has been devised to find the necessary model parameters from experimental data.

In future work, extended examples will be considered which include for example the effect of magnetization rotation on the strain response as well as the magnetization of MSMA materials. A constitutive model sufficient to handle such cases has been presented in this paper. The model will also be employed to predict the response to more complex loading paths. For example, the influence of magnetization rotation should be analyzed in an extended numerical example in which this effect is taken into account by utilizing the governing model equations (16) and (18). It would also be interesting to predict the mechanical detwinning and reorientation of MSMA martensite under constant magnetic fields, after the model parameters have been determined from an experiment of varying magnetic field under constant stress, such as done in this paper. With an appropriate inelastic strain tensor, this prediction can actually be handled by the model in its current form, a feature which illustrates that the presented formulation is not based on mere curve-fitting of available experimental data, but rather on the thermodynamically consistent derivation of constitutive equations from an appropriate energy expression, which also takes dissipative effects into account.

Note that no particular emphasis has been placed on the distinction between polycrystalline and single crystal material behavior. This is mainly due to the nature of the magneto-mechanical loading path considered in the numerical example. For mechanical loading paths resulting in multiaxial stress states, for example, the full elastic compliance tensor for tetragonal symmetry has to be considered for each of the martensitic variants. The influence of the single crystalline nature of the specimen used in experiments on constitutive modeling will be emphasized more strongly in future work.

Additional efforts will also be made in order to realize a more accurate prediction of the magnetization of the MSMA material, by investigating the evolution of the magnetic domain structure. Experimentally, this analysis could involve techniques such as Atomic Force Microscopy (AFM) or optical methods, for example the high resolution Interference-Contrast-Colloid (ICC) technique, as utilized by Sullivan and Chopra (2004). At this point it is not clear to which extent the rearrangement of the magnetic microstructure actually impacts the variant reorientation process, and the problem is still the subject of discussion in the research community. Some researchers have indicated that unfavorable magnetic domains are essentially eliminated at relatively low magnetic fields, as compared to the relevant field range of the experiment, (Tickle, 2000; O'Handley et al., 2003; O'Handley, 2004), while others attribute essential importance to the influence of the evolution of the magnetic domain structure on the variant reorientation process (Likhachev and Ullakko, 2000a; Hirsinger and Lexcellent, 2003b).

In a next step, the developed phenomenological constitutive model will be employed in solving magneto-mechanical boundary value problems. Experimental data could then be interpreted more accurately by considering the influence of specimen geometries. To this end, a proper formulation for the mechanics of magnetic continua must be considered, which includes Maxwell's equations, the balance laws of mass and momentum, the laws of thermodynamics as well as their coupling through the constitutive relations, mag-

netic forces, body couples, energy source terms as well as boundary and interface conditions. An interesting aspect may be the analysis of the influence of magnetic field gradient induced body forces on the magnetic shape memory effect.

Ongoing experimental research, in which experiments such as those described in this paper are conducted, is utilized to support the modeling of the magnetic shape memory effect (Karaman, 2004). This work is thereby not just restricted to the investigation of magnetically induced variant reorientation, but also the influence of externally applied magnetic fields on the martensitic phase transformation and thus on conventional shape memory and pseudoelastic behavior of MSMA. Additional experiments are also needed to obtain more conclusive evidence of the underlying microstructural mechanisms. Another important aspect of ongoing experimental research is concerned with finding alloys that exhibit higher blocking stress levels. Currently these stresses are less than 10 MPa, for the most common materials such as NiMnGa (Tickle and James, 1999), an unsatisfactory level for high force actuator design. More recently emerged material systems, for example CoNiAl (Karaca et al., 2003), have been investigated for the possibility of increased blocking stresses.

Acknowledgments

This work was supported by the Army Research Office, contract no. DAAD 19-02-1-0261 and the National Science Foundation, award no. CMS-0324537. The authors would also like to acknowledge the impact of the experimental MSMA work performed by Dr. Ibrahim Karaman and his group at the Mechanical Engineering Department at Texas A&M University on the modeling efforts presented in this paper. An extensive part of this manuscript was written during a visit to Prof. Hans Jürgen Maier's group at the Lehrstuhl für Werkstoffkunde, Universität Paderborn, as part of an ongoing research collaboration.

References

Bekker, A., Brinson, L. C., 1997. Temperature-induced phase transformation in a shape memory alloy: Phase diagram based kinetics approach. Journal of the Mechanics and Physics of Solids 45 (6), 949–988.

Bo, Z., Lagoudas, D. C., 1999. Thermomechanical modeling of polycrystalline SMAs under cyclic loading, Part I: Theoretical derivations. International Journal of Engineering Science 37, 1089–1140.

Boyd, J. G., Lagoudas, D. C., 1996. A thermodynamical constitutive model for shape memory materials. Part I. The monolithic shape memory alloy. International Journal of Plasticity 12 (6), 805–842.

Brinson, L. C., Huang, M. S., 1996. Simplifications and comparisons of shape memory alloy constitutive models. Journal of Intelligent Material Systems and Structures 7, 108–114.

Brown, Jr., W. F., 1966. Magnetoelastic Interactions. Vol. 9 of Tracts in Natural Philosophy. Springer-Verlag.

Cherechukin, A. A., Dikshtein, I. E., Ermakov, D. I., Glebov, A. V., Koledov, V. V., Kosolapov, D. A., Shavrov, V. G., Tulaikova, A. A., Krasnoperov, E. P., Takagi, T., 2001. Shape memory effect due to magnetic field-induced thermoelastic martensitic transformation in polycrystalline Ni-Mn-Fe-Ga alloy. Physics Letters A 291, 175–183.

Coleman, B. D., Gurtin, M. E., July 1967. Thermodynamics with internal state variables. The Journal of Chemical Physics 47 (2), 597–613.

Coleman, B. D., Noll, W., 1963. The thermodynamics of elastic materials with heat conduction and viscosity. Archive for Rational Mechanics and Analysis 13, 167–178.

Cui, J., Shield, T. W., James, R. D., 2004. Phase transformation and magnetic anisotropy of an iron-palladium ferromagnetic shape-memory alloy. Acta Materialia 52, 35–47.

Cullity, B. D., 1972. Introduction to Magnetic Materials. Addison-Wesley.

DeSimone, A., 1993. Energy minimizers for large ferromagnetic bodies. Archive for Rational Mechanics and Analysis 125, 99–143.

DeSimone, A., James, R., 2002. A constrained theory of magnetoelasticity. Journal of the Mechanics and Physics of Solids 50, 283–320.

DeSimone, A., James, R. D., 1997. A theory of magnetostriction oriented towards applications. Journal of Applied Physics 81 (8), 5706–5708.

DeSimone, A., James, R. D., 2003. Energetics of magnetoelastic domains in ferromagnetic shape memory alloys. Journal de Physique 112, 969–972.

Entchev, P. B., Lagoudas, D. C., 2001. Modeling porous shape memory alloys using micromechanical averaging techniques. Mechanics of Materials 34 (1), 1–24.

Eringen, A. C., Maugin, G. A., 1990a. Electrodynamics of Continua I — Foundations and Solid Media. Springer-Verlag.

Eringen, A. C., Maugin, G. A., 1990b. Electrodynamics of Continua II — Fluids and Complex Media. Springer-Verlag.

Fujita, A., Fukamichi, K., Gejima, F., Kainuma, R., Ishida, K., 2000. Magnetic properties and large magnetic-field-induced strains in off-stoichiometric Ni-Mn-Al heusler alloys. Applied Physics Letters 77 (19), 3054–3056.

Glavatska, N. I., Rudenko, A. A., Glavatskiy, I. N., L'vov, V. A., 2003. Statistical model of magnetostrain effect in martensite. Journal of Magnetism and Magnetic Materials 265 (2), 142–151.

Govindjee, S., Hall, G. J., 2000. A computational model for shape memory alloys. International Journal of Solids and Structures 37 (5), 735–760.

Hirsinger, L., Lexcellent, C., 2003a. Internal variable model for magneto-mechanical behaviour of ferromagnetic shape memory alloys Ni-Mn-Ga. Journal de Physique IV 112, 977–980.

Hirsinger, L., Lexcellent, C., 2003b. Modelling detwinning of martensite platelets under magnetic and (or) stress actions on NiMnGa alloys. Journal of Magnetism and Magnetic Materials 254–255, 275–277.

Hutter, K., van de Ven, A. A. F., 1978. Field Matter Interactions in Thermoelastic Solids. Vol. 88 of Lecture Notes in Physics. Springer-Verlag.

James, R. D., Hane, K. F., 2000. Martensitic transformations and shape-memory materials. Acta Materialia 48 (1), 197–222.

James, R. D., Wuttig, M., 1996. Alternatice smart materials. Proceedings of SPIE, Symposium on Smart Structures and Materials 2715, 420–426.

James, R. D., Wuttig, M., 1998. Magnetostriction of martensite. Philosophical Magazine A 77 (5), 1273–1299.

Jeong, S., Inoue, K., Inoue, S., Koterazawa, K., Taya, M., Inoue, K., 2003. Effect of magnetic field on martensite transformation in a polycrystalline Ni_2MnGa. Material Science & Engineering A 359, 253–260.

Kakeshita, T., Takeuchi, T., Fukuda, T., Tsujiguchi, M., Saburi, T., Oshima, R., Muto, S., 2000. Giant magnetostriction in an ordered Fe_3Pt single crystal exhibiting a martensitic transformation. Applied Physics Letters 77 (10), 1502–1504.

Karaca, H. E., Karaman, I., Lagoudas, D. C., Maier, H. J., Chumlyakov, Y. I., 2003. Recoverable stress-induced martensitic transformation in a ferromagnetic CoNiAl alloy. Scripta Materialia 49, 831–836.

Karaman, I., 2004. Thermo-magneto-mechanical characterization and testing of MSMA single crystals, conducted at Texas A&M University, Departments of Aerospace Engineering and Mechanical Engineering. Internal Correspondence.

Kiang, J., Tong, L., 2005. Modelling of magneto-mechanical behavior of Ni-Mn-Ga single crystals. To be published in Journal of Magnetism and Magnetic Materials XX (x), 1–19.

Kiefer, B., Lagoudas, D. C., 2004. Phenomenological modeling of ferromagnetic shape memory alloys. Proceedings of SPIE, Smart Structures and Materials: Active Materials: Behavior and Mechanics, San Diego, CA, 14–18 March 2004. Vol. 5387, 164–176.

Kiefer, B., Lagoudas, D. C., 2005. Modeling of the magnetic field-induced martensitic variant reorientation and the associated magnetic shape memory effect in msmas. Proceedings of SPIE, Smart Structures and Materials: Active Materials: Behavior and Mechanics, San Diego, CA, 6–10 March 2005. Vol. 5761, xxx–xxx.

Kittel, C., 1949. Physical theory of ferromagnetic domains. Reviews of Modern Physics 21 (4), 541–583.

Kittel, C., Galt, J. K., 1956. Ferromagnetic domain theory. Solid State Physics 3, 437–564.

Lagoudas, D. C., Bo, Z., 1999. Thermomechanical modeling of polycrystalline SMAs under cyclic loading, Part II: Material characterization and experimental results for a stable transformation cycle. International Journal of Engineering Science 37, 1141–1173.

Lagoudas, D. C., Bo, Z., Qidwai, M. A., 1996. A unified thermodynamic constitutive model for SMA and finite element analysis of active metal matrix composites. Mechanics of Composite Materials and Structures 3, 153–179.

Leclercq, S., Lexcellent, C., 1996. A general macroscopic description of the thermomechanical behavior of shape memory alloys. Journal of the Mechanics and Physics of Solids 44 (6), 953–980.

Liang, C., Rogers, C. A., 1990. One-dimensional thermomechanical constitutive relations for shape memory materials. Journal of Intelligent Material Systems and Structures 1, 207–234.

Liang, Y., Wada, T., Tagawa, T., Taya, M., 2002. Model calculation of stress-strain relationship of polycrystalline Fe-Pd and 3D phase transformation diagram of ferromagnetic shape memory alloys. Proceedings of SPIE, Smart Structures and Materials 2002: Active Materials: Behavior and Mechanics, San Diego, CA, March 18–21, Vol. 4699, 206–216.

Likhachev, A. A., Ullakko, K., 2000a. Magnetic-field-controlled twin boundaries motion and giant magneto-mechanical effects in Ni-Mn-Ga shape memory alloy. Physics Letters A 275, 142–151.

Likhachev, A. A., Ullakko, K., 2000b. Quantitative model of large magnetostrain effect in ferromagnetic shape memory alloys. The European Physical Journal B 14 (2), 263–267.

Lubliner, J., Auricchio, F., 1996. Generalized plasticity and shape memory alloys. International Journal of Solids and Structures 33 (7), 991–1003.

Malvern, L. E., 1969. Introduction to the Mechanics of a Continuous Medium. Series in Engineering of the Physical Sciences. Prentice Hall.

Marioni, M. A., O'Handley, R. C., Allen, S. A., 2002. Analytical model for field-induced strain in ferromagnetic shape-memory alloy polycrystals. Journal of Applied Physics 91 (10), 7807–7809.

Maugin, A. G., 1999. The Thermodynamics of Nonlinear Irreversible Behaviors. Vol. 27 of Nonlinear Science, Series A. World Scientific.

Morito, H., Fujita, A., Kainuma, R., Ishida, K., Oikawa, K., 2002. Magnetocrystalline anisotropy in single-crystal Co-Ni-Al ferromagnetic shape-memory alloy. Applied Physics Letters 81 (9), 1657–1659.

Muellner, P., Chernenko, V. A., Kostorz, G., 2003. A microscopic approach to the magnetic-field-induced deformation of martensite (magnetoplasticity). Journal of Magnetism and Magnetic Materials 267, 325–334.

Murray, S. J., Farinelli, M., Kantner, C., Huang, J. K., Allen, A. M., O'Handley, R. C., 1998. Field-induced strain under load in Ni-Mn-Ga magnetic shape memory materials. Journal of Applied Physics 83 (11), 7297–7299.

Murray, S. J., Hayashi, R., Marioni, M., Allen, S. M., O'Handley, R. C., 1999. Magnetic and mechanical properties of FeNiCoTi and NiMnGa magnetic shape memory alloys. Proceedings of SPIE 3675, 204–211.

Murray, S. J., Marioni, M., Allen, S. M., O'Handley, R. C., 2000a. 6% magnetic-field-induced strain by twin-boundary motion in ferromagnetic Ni-Mn-Ga. Applied Physics Letters 77 (6), 886–888.

Murray, S. J., Marioni, M., Kukla, A. M., Robinson, J., O'Handley, R. C., Allen, S. M., 2000b. Large field induced strain in single crystalline Ni-Mn-Ga ferromagnetic shape memory alloy. Journal of Applied Physics 87 (9), 5774–5776.

Murray, S. J., O'Handley, R. C., Allen, S. M., 2001. Model for discontinuous actuation of ferromagnetic shape memory alloy under stress. Journal of Applied Physics 89 (2), 1295–1301.

O'Handley, R. C., 1998. Model for strain and magnetization in magnetic shape-memory alloys. Journal of Applied Physics 83 (6), 3263–3270.

O'Handley, R. C., 2000. Modern Magnetic Materials. John Wiley & Sons.

O'Handley, R. C., 14–18 March 2004. Privat technical discussion. SPIE, 11th Annual International Symposium: Smart Structures and Materials, San Diego, CA.

O'Handley, R. C., Allen, S. M., Paul, D. I., Henry, C. P., Marioni, M., Bono, D., Jenkins, C., Banful, A., Wager, R., 2003. Keynote address: Magnetic field-induced strain in single crystal Ni-Mn-Ga. Proceedings of SPIE, Symposium on Smart Structures and Materials 5053, 200–206.

Pao, Y. H., Hutter, K., 1975. Electrodynamics for moving elastic solids and viscous fluids. Proceedings of the IEEE 63 (7), 1011–1021.

Patoor, E., Eberhardt, A., Berveiller, M., 1996. Micromechanical modelling of superelasticity in shape memory alloys. Journal de Physique IV 6, C1—277–292.

Penfield Jr., P., Haus, H. A., 1967. Electrodynamics of Moving Media. Vol. 40 of Research Monographs. MIT Press.

Qidwai, M. A., Lagoudas, D. C., 2000a. Numerical impementation of a shape memory alloy thermomechanical constitutive model using return mapping algorithms. International Journal for Numerical Methods in Engineering 47, 1123–1168.

Qidwai, M. A., Lagoudas, D. C., 2000b. On the thermodynamics and transformation surfaces of polycrystalline NiTi shape memory alloy material. International Journal of Plasticity 16, 1309–1343.

Sato, Y., Tanaka, K., 1988. Estimation of energy dissipation in alloys due to stress-induced martensitic transformation. Res Mechanica 23, 381–392.

Shield, T. W., 2003. Magnetomechanical testing machine for ferromagnetic shape-memory alloys. Review of Scientific Instruments 74 (9), 4077–4088.

Shu, S. G., Lagoudas, D. C., Hughes, D., Wen, J. T., 1997. Modeling of a flexible beam actuated by shape memory alloy wires. Smart Materials and Structures 6, 265–277.

Sozinov, A., Likhachev, A. A., Lanska, N., Söderberg, O., Ullakko, K., Lindroos, V. K., 2003. Effect of crystal structure on magnetic-field-induced strain in Ni-Mn-Ga. Proceedings of SPIE, Symposium on Smart Structures and Materials 5053, 586–594.

Spaldin, N. A., 2003. Magnetic Materials: Fundamentals and Device Applications. Cambridge University Press.

Sullivan, M. R., Chopra, H. D., 2004. Temperature- and field-dependent evolution of micromagnetic structure in ferromagnetic shape-memory-alloys. Physical Review B 70, 094427–(1–8).

Tanaka, K., 1986. A thermomechanical sketch of shape memory effect: One-dimensional tensile behavior. Res Mechanica 18, 251–263.

Tickle, R., May 2000. Ferromagnetic shape memory materials. Ph.D. thesis, University of Minnesota.

Tickle, R., James, R. D., 1999. Magnetic and magnetomechanical properties of Ni_2MnGa. Journal of Magnetism and Magnetic Materials 195 (3), 627–638.

Tickle, R., James, R. D., Shield, T., Schumacher, P., Wuttig, M., Kokorin, V. V., 1999. Ferromagnetic shape memory in the NiMnGa system. IEEE Transactions on Magnetics 35 (5), 4301–4310.

Tiersten, H. F., 1964. Coupled magnetomechanical equations for magnetically saturated insulators. Journal of Mathematical Physics 5 (9), 1298–1318.

Truesdell, C., Toupin, R., 1960. Principles of Classical Mechanics and Field Theory. Vol. III/1 of Encyclopedia of Physics. Springer-Verlag, Ch. The Classical Field Theories, pp. 226–795.

Ullakko, K., Ezer, Y., Sozinov, A., Kimmel, G., Yakovenko, P., Lindroos, V. K., 2001. Magnetic-field-induced strains in polycrystalline Ni-Mn-Ga at room temperature. Scripta Materialia 44, 475–480.

Ullakko, K., Huang, J. K., Kantner, C., O'Handley, R. C., Kokorin, V. V., 1996. Large magnetic-field-induced strains in Ni_2MnGa single crystals. Applied Physics Letters 69 (13), 1966–1968.

Wada, T., Liang, Y., Kato, H., Tagawa, T., Taya, M., Mori, T., 2003. Structural change and straining in Fe-Pd polycrystals by magnetic field. Material Science & Engineering A 361, 75–82.

Webster, P. J., Ziebeck, K. R. A., Town, S. L., Peak, M. S., 1984. Magnetic order and phase transformation in Ni_2MnGa. Philosophical Magazine B 49 (3), 295–310.

Wuttig, M., Li, J., Craciunescu, C., 2001. A new ferromagnetic shape memory alloys system. Scripta Materialia 44, 2393–2397.

Wuttig, M., Liu, L., Tsuchiya, K., James, R. D., 2000. Occurrence of ferromagnetic shape memory alloys (invited). Journal of Applied Physics 87 (9), 4707–4711.

Yamamoto, T., Taya, M., Sutou, Y., Liang, Y., Wada, T., Sorensen, L., 2004. Magnetic field-induced reversible variant rearrangement in Fe-Pd single crystals. Acta Materialia 52 (17), 5083–5091.

Zasimchuk, I. K., Kokorin, V. V., Martynov, V. V., Tkachenko, A. V., Chernenko, V. A., 1990. Crystal structure of martensite in Heusler alloy Ni_2MnGa. Physics of Metals and Metallography 69 (6), 104–108.